Title:

Altered *N*-glycan composition impacts flagella mediated adhesion in *Chlamydomonas reinhardtii*

Short title:

N-glycosylation impacts adhesion in *Chlamydomonas*

Abstract

For the unicellular alga *Chlamydomonas reinhardtii*, the presence of *N*-glycosylated proteins on the surface of two flagella is crucial for both cell-cell interaction during mating and flagellar surface adhesion. However, it is not known whether only the presence or also the composition of *N*-glycans attached to respective proteins is important for these processes. To this end, we tested several *C. reinhardtii* insertional mutants and a CRIPSR/Cas9 knockout mutant of xylosyltransferase 1A, all possessing altered *N*-glycan compositions. Taking advantage of atomic force microscopy and micropipette force measurements, our data revealed that reduction in *N*-glycan complexity impedes the adhesion force required for binding the flagella to surfaces as demonstrated by force spectroscopy and impairs polystyrene bead binding and transport. Notably, assembly, intraflagellar transport and protein import into flagella are not affected by altered *N*-glycosylation. Thus, we conclude that proper *N*-glycosylation of flagellar proteins is crucial for adhering *C. reinhardtii* cells onto surfaces, indicating that *N*-glycans mediate surface adhesion via direct surface contact.

Keywords

adhesion/ AFM/ C. reinhardtii/ flagella/ *N*-glycosylation

Introduction

N-glycosylation, as one of the major post-translational modifications, takes place along the ER/Golgi secretion route and consequently most *N*-linked glycans are found on proteins facing

the extracellular space. Initial steps of *N*-glycosylation in the ER are highly conserved among most eukaryotes and consist of the synthesis of a common prebuilt *N*-glycan precursor onto a dolichol phosphate. Following the transfer of the glycan precursor onto the asparagine of the consensus sequence N-X-S/T of a nascent protein (where X can be any amino acid except proline), the glycoprotein is folded by the glycan recognizing chaperones Calnexin and Calreticulin (Stanley P, Taniguchi N, 2017). Subsequent *N*-glycan maturation steps in the Golgi are species dependent and give rise to a high variety of *N*-glycan structures. In land plants, Golgi maturation leads to *N*-glycans modified with β1,2-core xylose and α1,3-core fucose (Strasser, 2016). In *Chlamydomonas reinhardtii*, a unicellular biflagellate green alga, *N*-glycans can be decorated with core xylose and -fucose (Lucas et al., 2020; Oltmanns et al., 2020; Schulze et al., 2018). Additionally, *6O*-methylation of mannose and addition of a terminally linked β1,4-xylose were reported (Mathieu-Rivet et al., 2013). While the functional advantage of *N*-linked glycans to mature proteins is hardly understood, it is known that blocking the synthesis of a full *N*-glycan precursor results in hypoglycosylated proteins that cannot be folded properly (Gardner et al., 2013). Instead, they are degraded via the ER-associated degradation pathway (ERAD) and are consequently not targeted correctly (Adams et al., 2019; Cherepanova et al., 2016). Therefore, impairment of glycosylation at such early stage is lethal in both uni- and multi-cellular organisms and only when inhibition of glycosylation is carefully dosed (e.g. by tunicamycin), immediate physiological effects caused by hypoglycosylation can be observed (Kukuruzinska et al., 1987). Looking at *C. reinhardtii*, treatment of vegetative cells with tunicamycin lead to an impaired flagellar adhesiveness, indicating that glycoproteins are crucial for adhesion and the subsequent onset of gliding (Bloodgood, 1982). However, whether this phenotype is linked to mistargeting of proteins due to hypoglycosylation and/or the lack of *N*-glycans on the flagella surface is unclear.

Whole cell gliding is one of two flagella based motilities in *C. reinhardtii* besides swimming (Ishikawa and Marshall, 2011; Kozminski et al., 1993; Snell et al., 2004). In principle, the cell adheres to a surface via its flagella, positioning them in a 180° angle and initiates gliding along the solid or semisolid surface into the direction in which one flagellum is pointing (designating it as leading flagellum) (Bloodgood, 2009). Interestingly, flagella not only bind to large solid surfaces, but they also bind to small, inert objects (e.g. polystyrene microbeads) that are moved along the flagellar membrane. While the two events, summarized as flagellar membrane motility, are believed to underly the same molecular machinery, it is assumed that they start with an adhesion of flagella membrane components to the surface (Bloodgood and Salomonsky, 1998). A micropipette force measurement approach recently showed that the flagella adhesion forces on different model surfaces with tailored properties lie in the range of 1 to 4 nN and that only positive surface charge diminished the adhesion force significantly (Backholm and Bäumchen, 2019; Kreis et al., 2019, 2018). Remarkably, surface iodination experiments in the early 1980s revealed a single protein called flagellar membrane glycoprotein 1B (FMG-1B) as the main player mediating surface contact (Bloodgood and Workman, 1984). FMG-1B is exclusively located in the flagellar membrane and has a remarkable size of around 350 kDa (4389 amino acids) with a large extra-flagellar part (4340 amino acids) anchored in the membrane via a single predicted trans membrane helix of 22 amino acids (Bloodgood et al., 2019). As the name indicates, it is heavily *N*- and *O*-glycosylated. A recent knock down study showed, that it is the main constituent of the glycocalyx surrounding the flagellum. Additionally, a *fmg-1B* mutant showed a drastically reduced ability to glide (Bloodgood et al., 2019). Strikingly, FMG-1B is present at a high copy number and turns over rapidly within approximately 1 h (Bloodgood, 2009). The rapid turnover is probably attributed to the fact that flagellar membrane components are constantly shed into the medium as flagellar ectosomes (Bloodgood, 2009; Wood et al., 2013). FMG-1B and another *N*-glycosylated membrane

component, FAP113, have been shown to be eventually torn out of the membrane once bound to microbeads (Kamiya et al., 2018). Whether FAP113 is only involved in microbead binding or also in whole cell gliding is unknown.

Recently, it was found that flagellar adhesion to surfaces is switchable by light, indicating that a blue-light photoreceptor signal is governing this process (Kreis et al. 2018). Following adhesion to the surface, a transmembrane signal mediates translation of the adhesion event into a calcium transient and protein phosphorylation cascade (Bloodgood, 2009; Collingridge et al., 2013; Kreis et al., 2018). According to the current model, an interaction of the short cytoplasmic part of FMG-1B with Intraflagellar Transport (IFT) may occur (Laib et al., 2009; Shih et al., 2013). IFT moves bidirectionally along the flagellar microtubules, the anterograde transport is driven by kinesin 2 and retrograde transport is driven by cytoplasmic dynein-1b (Cole et al., 1998; Huangfu et al., 2003; Kozminski et al., 1995; Lechtreck, 2015; Pedersen and Rosenbaum, 2008; Porter et al., 1999; Rosenbaum and Witman, 2002). Since retrograde motor dynein-1b pauses relative to the adhesion site while FMG-1B tethers to the solid surface through its large extracellular carbohydrate domain (Bloodgood, 2009), the force generated by motor proteins will push the microtubule into the opposite direction, dragging the cell body and the second flagellum behind; the gliding process is initiated (Shih et al., 2013).

Considering that *N*-glycoproteins *per se* are important for adhesion but are constantly lost from the flagellar membrane, gliding is supposed to require an enormous amount of energy, which suggests that flagella mediated adhesion has a somewhat high importance. Furthermore, it opens the question whether the maturation of *N*-glycans (as additional energy expense) in Golgi is important for flagella mediated adhesion, i.e. whether *N*-glycosylation is crucial for adhesion beyond proper glycoprotein folding. Therefore, we compared flagellar membrane motility of different mutant strains impaired in *N*-glycan maturation (characterized in Schulze *et al.* 2018).

We found that *N*-glycan maturation indeed impacts the interaction of flagellum and surface in all mutants analyzed.

Results

Altered *N*-linked glycans do not change the flagellar localization of FMG-1B

To test whether *N*-glycan maturation in Golgi is important for flagellar surface motility in *C. reinhardtii*, two insertional mutants such as IM$_{Man1A}$, IM$_{XylT1A}$ and their double mutant IM$_{Man1A}$xIM$_{XylT1A}$ were studied. Initially, these mutants had been described in Schulze *et al.* 2018, where *N*-glycan patterns of supernatant proteins were analyzed and compared (Fig. 1A). The insertional mutagenesis giving rise to these mutants was performed in the parental strain CC-4375 (a *ift46* mutant backcrossed with CC-124) complemented with IFT-46::YFP, referred to as WT-Ins throughout the current study. The first mutant, deficient in xylosyltransferase 1A (IM$_{XylT1A}$), produces *N*-glycans devoid of core xylose while simultaneously having a reduced length. Second mutant IM$_{Man1A}$, a knock down mutant of mannosidase 1A, is mainly characterized by a lack of 6*O*-methylation of mannose residues while the *N*-glycan length is slightly greater than in WT-Ins. Furthermore, *N*-glycans of IM$_{Man1A}$ are slightly reduced in terminal xylose and core fucose. Finally, a double mutant of the above two single mutants (IM$_{Man1A}$xIM$_{XylT1A}$, obtained by genetic crossing) produces *N*-glycans devoid of 6*O*-methylation but of WT-Ins length and carrying core xylose and fucose residues (Fig. 1A). It is of note that in none of the mutants the flagellar length is altered as compared to WT-Ins (Figure 1 - Supplementary Fig. 1). To confirm that flagellar *N*-glycan patterns of these mutants deviate from WT-Ins, whole cell extracts and isolated flagella were probed with anti-HRP, binding to β1,2-xylose and α1,3-fucose attached to the *N*-glycan core (Kaulfürst-Soboll et al., 2011). In line with previous publications, the antibody showed a higher affinity towards *N*-glycoproteins synthesized by IM$_{Man1A}$ and IM$_{Man1A}$xIM$_{XylT1A}$ while it showed a decreased affinity towards

probes of IM*XylT1A* (Figure 1 - Supplementary Fig. 2) (Schulze et al., 2018). Further lectin-affino blotting with concanavalin A (ConA) was performed on whole cell extracts, revealing increased ConA-affinity in all three *N*-glycosylation mutants compared to WT-ins (Figure 1 – Supplementary Fig.3).

Since FMG-1B is the major constituent of the flagellar glycoproteome and to date the only protein proven to be involved in flagellar surface motility, different monoclonal antibodies raised against FMG-1B were employed to analyze FMG-1B localization (Bloodgood et al., 1986; Long et al., 2016). The whole cell extracts or isolated flagella from IM*Man1A*, IM*XylT1A* and their double mutant IM*Man1A*xIM*XylT1A* were probed separately with the glycan epitope recognizing antibody or the antibody against the protein backbone of FMG-1B. FMG-1B was found in whole cells and flagella of WT-Ins and all three mutants. Hereby, the protein amount was similar in all four strains as indicated by the use of the FMG-1B protein specific antibody (Fig. 1B). Contrarily, the antibody raised against FMG-1B glycan epitopes barely detected whole cell or flagella probes of IM*Man1A* and IM*Man1A*xIM*XylT1A*. Also, the FMG-1B glycan signal decreased in the mutant IM*XylT1A*, particularly in the whole cell sample. Taken together, these immuno-blots confirm that the *N*-glycan pattern of FMG-1B is altered in the mutants, while the protein localization is not affected by this alteration. In addition, label free mass spectrometric quantification confirmed that FMG-1B is correctly targeted to the flagella in all mutants analyzed (Fig. 1 C). The same is true for FAP113, another protein shown to be involved in flagella surface motility (Fig. 1D).

To compare the localization of glycan and protein of FMG1-B in WT-Ins and mutants, the cells were immuno-stained with the two FMG-1B specific antibodies described above. A uniform signal of the glycan specific antibody was found in the flagella and the cell wall of WT-Ins (Fig. 1E, left panel). It should be noted, that such cross reaction with cell wall localized glycosylated

proteins has been reported previously (Bloodgood et al., 1986). In line with the immuno-blotting experiment, no glycan signal was observed in the flagella or cell wall of IM$_{Man1A}$ and the double mutant, while signal intensity was low in the flagella of mutant IM$_{XylT1A}$ (Fig.1E, left panel and). The faint FMG-1B signal in IM$_{XylT1A}$ compared to the WT-Ins was clearly observed when WT-Ins and IM$_{XylT1A}$ were mixed prior to immuno-staining (Figure 1 – Supplementary Fig.6). When the FMG-1B peptide antibody was used, an uniform signal is found in the flagella of WT-ins, M$_{Man1A}$, IM$_{XylT1A}$ and the mutant IM$_{Man1A}$xIM$_{XylT1A}$ (Fig. 1E, right panel). In summary, these data show that altered *N*-glycan maturation did not affect the flagellar localization of FMG-1B. Although FMG-1B is the most prominent and best studied flagella membrane glycoprotein, there might be other glycoproteins involved in flagellar adhesion. Nevertheless, no protein was found consistently and significantly changed in abundance in flagella of the IM strains analyzed when compared to WT-Ins (Figure 1 - Supplementary Fig. 7), also indicating that flagellar assembly is not considerably altered in the mutants versus WT.

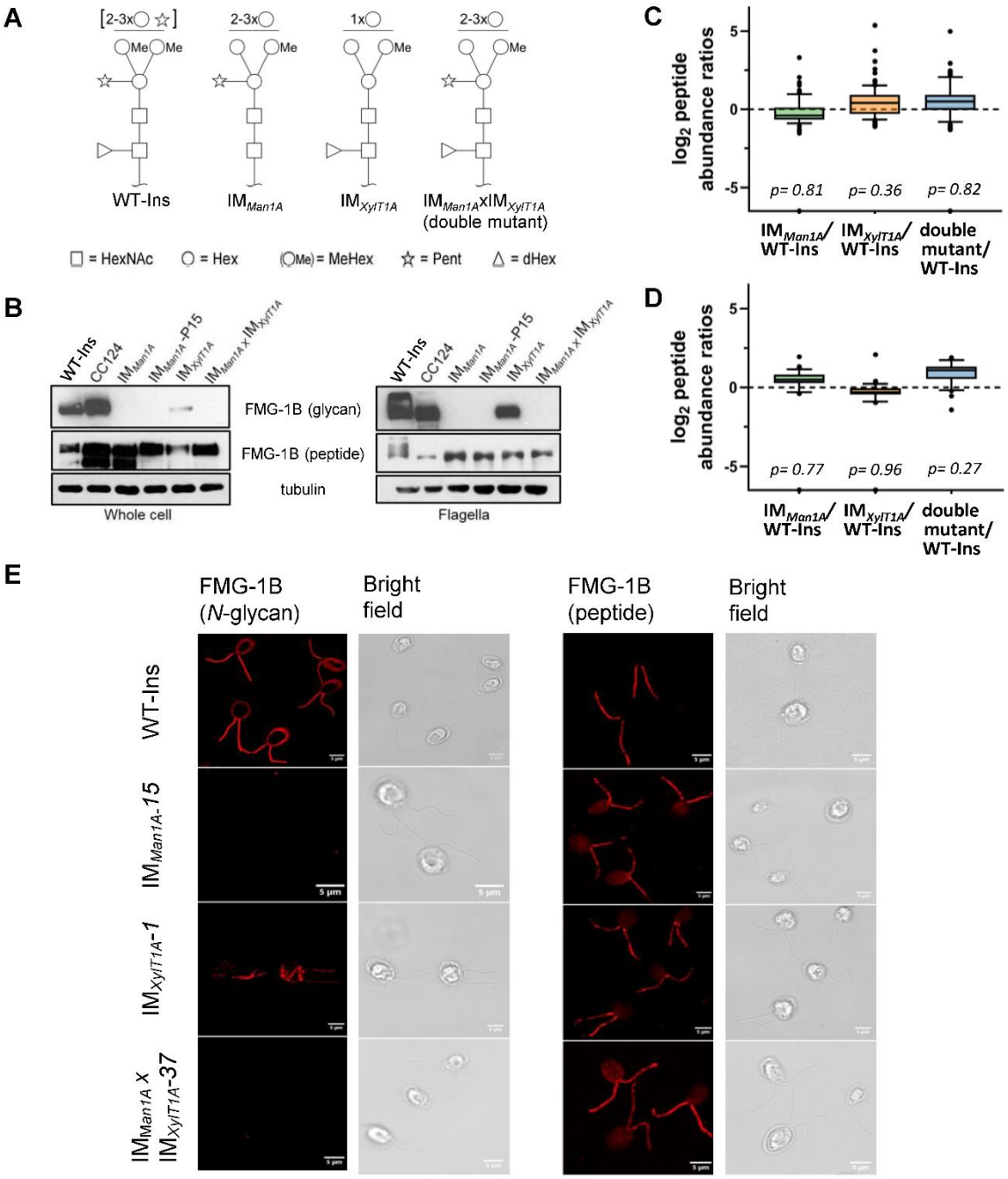

Figure 1. Altered *N*-glycosylation of FMG-1B does not change its flagellar localization

A, Diagram of *N*-linked glycan compositions of mutant strains characterized in Schulze *et al.* 2018 and used in the current study. While IM_{Man1A} and the double mutant are mainly characterized by a lower degree of methylation (Me), *N*-glycans of IM_{XylT1A} are decreased in length and lack the core xylose. All monosaccharides depicted above the horizontal line can be bound to any subjacent residue or to any residue at the same level. Square: *N*-Acetylglucosamine, Circe: hexose, Triangle: fucose, Star: xylose). B, Probing whole cell and flagella samples with antibodies directed against *N*-glycans or the protein

backbone of FMG-1B.(Bloodgood et al., 1986) C, Log2 peptide abundances of FMG-1B obtained by label free MS analysis. D, Log2 peptide abundances of FAP-113 obtained by label free MS analysis. E, Immuno staining of WT-Ins mutant cells (IM_{Man1A}, IM_{XylT1A} or IM_{Man1A}xIM_{XylT1A}) with antibodies directed against FMG-1B. IM_{Man1A}, IM_{XylT1A} or IM_{Man1A}xIM_{XylT1A} express IFT46::YFP. To prevent YFP signal to interfere in immune staining and allow direct comparison of signal in WT-Ins and mutants, strains were crossed with WT-CC124 and progenies of IM_{Man1A}, IM_{XylT1A} or IM_{Man1A}xIM_{XylT1A} absent of IFT46::YFP (#37, #1 and #15) used for immune staining experiments (see Figure 1 – Supplementary Fig. 5)

Altered *N*-linked glycans attenuate bead attachment to and movement along the flagellar membrane

In *C. reinhardtii,* polystyrene microspheres adhere to and move bidirectionally along the flagellar surface (Bloodgood, 1981). To check the effect of altered *N*-glycans on these processes, beads with a diameter of 0.7 μm were added to cell suspensions of IM_{Man1A}, IM_{XylT1A} and the double mutant and the number of beads attached to- or moved along flagella were quantified (Fig. 2A and B, exemplary video in Figure 2 - Video 1). In WT-Ins strains, about 52 % of all flagella had at least one bead attached, whereas the percentage of flagella with beads bound decreased to 46 % in IM_{Man1A}, 33 % in IM_{XylT1A} and 27 % in the double mutant (Fig. 2A). Among the beads attached, 37 % moved along flagella of WT-Ins, 22 % in IM_{Man1A}, 29 % in IM_{XylT1A} and 27 % in the double mutant (Fig. 2B). These data suggested that interaction of flagellar membrane and surface is altered due to altered *N*-glycan composition in these mutants.

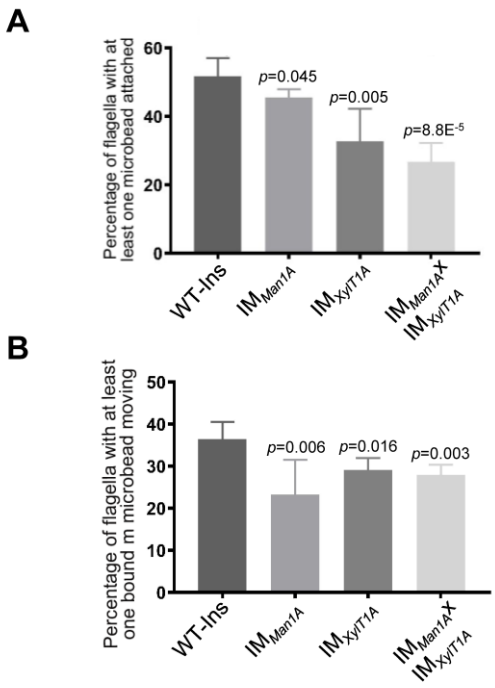

Figure 2. Altered *N*-glycosylation diminishes flagellar polystyrene bead attachment and -transport.

A, Percentage of flagella with at least one polystyrene bead bound. Cells were incubated with polystyrene beads (0.7 µm in diameter) and subsequently analyzed by light microscopy. B, Percentage of polystyrene beads transported along the flagellum with at least one polystyrene bead bound. Results present mean of three replicates with 50 cells analyzed per replicate. Error bars show SEM of three replicates. T-test was used for statistical analysis.

Quantification of the flagella mediated adhesion using atomic force microscopy

Flagella mediated surface adhesion force was measured via atomic force microscopy (AFM) (Fig. 3A). Here, cells adhered to a cover slide were attached to an AFM cantilever via physical contact (Liu et al., 2011). Subsequently, the AFM cantilever was pulled upwards and the force required to pull the cells was recorded (Fig. 3B). To inhibit whole-cell gliding during the measurement, ciliobrevin D was used to inhibit dynein-1b activity and consequently the cell gliding (Firestone et al., 2012). Remarkably, the forces necessary to overcome the adhesion of *C. reinhardtii* flagella to the surface were significantly reduced in these three mutants analyzed

as compared to WT-Ins (Fig. 3B and C). Especially in the double mutant the adhesion force was reduced from 8 nN in WT-Ins to 1 nN, while the average energy was reduced from 4 to 0.5 J nm^{-1} (Fig. 3C and D). This result indicates that an altered *N*-glycan composition impacts the flagellar adhesion force onto a solid substrate.

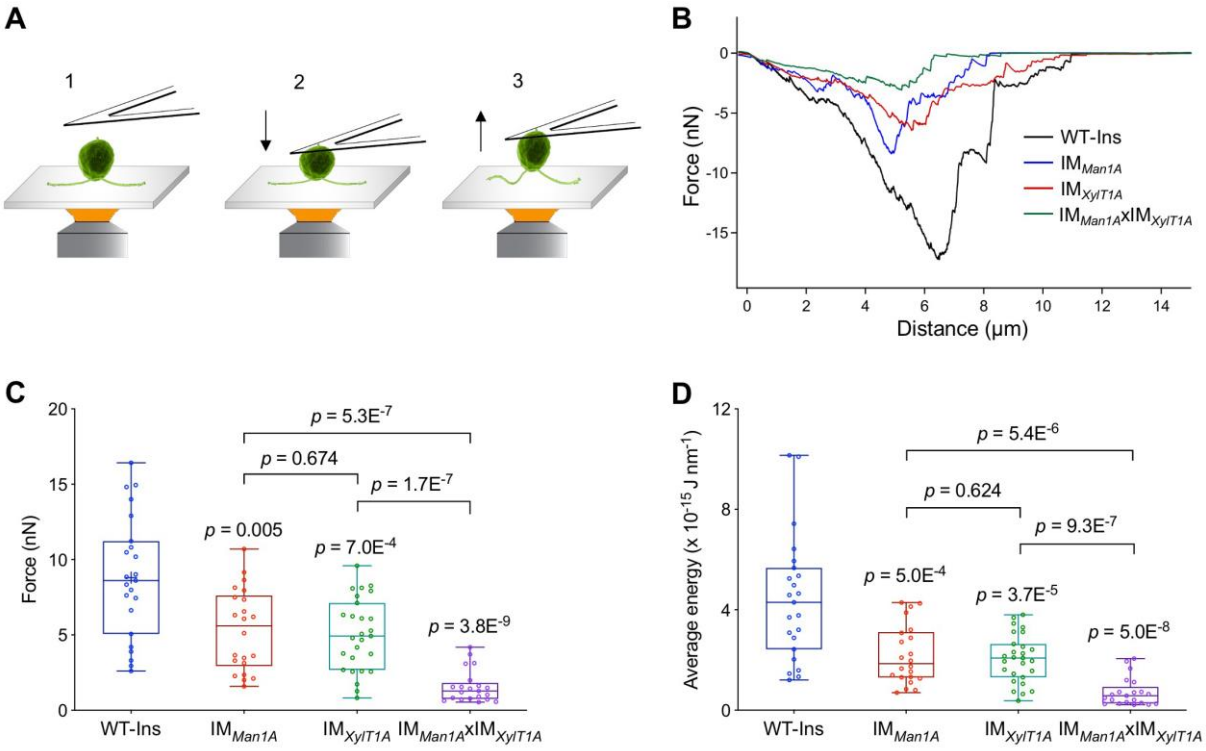

Figure 3. Quantification of the flagella-mediated adhesion using atomic force microscopy.

A, Diagram of experimental procedures for force measurement: the cell adhered to the surface (1); the cell attached to the AFM cantilever (2); the cell was pulled up from the surface by AFM cantilever (3). Please note, that retrograde IFT, i.e. gliding was inhibited by ciliobrevin D during all measurements presented here. B, Representative force curves acquired for strains including WT, IM$_{Man1A}$, IM$_{XylT1A}$ and IM$_{Man1A}$xIM$_{XylT1A}$. C, Flagella adhesion forces of WT-Ins, IM$_{Man1A}$, IM$_{XylT1A}$ and IM$_{Man1A}$xIM$_{XylT1A}$ were generated from force curves (B). D, Average energy of flagellar adhesion of WT-Ins, IM$_{Man1A}$, IM$_{XylT1A}$ and IM$_{Man1A}$xIM$_{XylT1A}$. Three biological replicates were performed with minimum 5 cells measured per replicate. The p-values are obtained from a two-sided, two sample t-test of mean values.

Quantification of flagellar adhesion using a micropipette force measurement approach

To validate the AFM adhesion force measurements, an independent *in vivo* force measurement approach (Backholm and Bäumchen, 2019; Kreis et al., 2018) was used with another genetic background mutant, xylosyltransferase 1A (CRISPR$_{XylT1A_1}$) , generated in parental wildtype SAG11-32b (WT-SAG) by employing CRISPR/Cas9 (Figure 4 - Supplementary Fig. 1). As a wavelength dependency of flagellar adhesion had been revealed using this approach (Backholm and Bäumchen, 2019), adhesion forces of the same cells were measured under precisely controlled blue- and red-light conditions using a micropipette adhesion force measurement approach. Adhesion forces were measured in presence and absence of dynein-1b inhibitor ciliobrevin D. Importantly, adhesion forces in CRISPR$_{XylT1A_1}$ were significantly diminished in comparison to respective WT under both ciliobrevin D conditions confirming AFM results (Fig. 4). Illuminating cells with red light dramatically decreased the adhesion force in both WT-SAG and CRISPR$_{XylT1A_1}$ in presence as well as in absence of ciliobrevin D. Notably, removal of ciliobrevin D resulted in a significant decrease in adhesion force for both WT-SAG and CRISPR$_{XylT1A_1}$ from ~ 2.6 nN to ~1.3 nN in WT-SAG and from ~ 1.8 nN to ~1 nN in CRISPR$_{XylT1A_1}$.

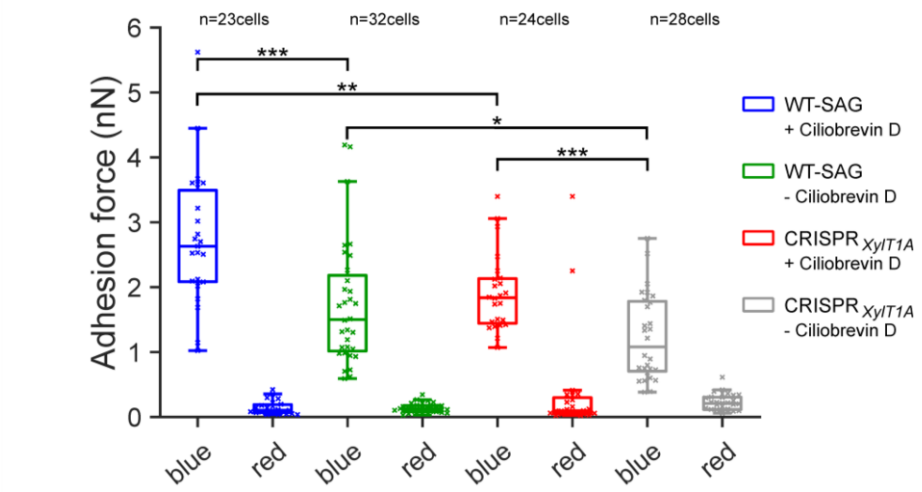

235

236

237 **Figure 4. Assessing flagella adhesion forces using micropipette force microscopy.**

238 Flagella mediated adhesion forces acquired for WT-SAG and a xylosyltransferase 1A mutant generated
239 in the genetic background of WT-SAG (CRISPR$_{XylT1A_1}$). Micropipette force measurements of the
240 same cells were performed for both strains under blue and red light in the (+) presence or (-) absence
241 of ciliobrevin D. Mean values of 10 measurements per cell are depicted, statistical analysis was
242 performed on mean values. The p-values obtained a from Kolmogorov-Smirnov test are respectively
243 (from top to bottom): (***) p=0.0004, (**) p=0.0016, (*) p=0.0491, (***) p=0.0009.

244

245 **The effect of altered *N*-glycosylation on IFT and gliding**

246 As presented in Figure 3, the strongest effect on adhesion forces assessed was observed in the
247 double mutant IM$_{Man1A}$xIM$_{XylT1A}$ when compared to WT-Ins. In the absence of ciliobrevin D,
248 the adhesion force measured by AFM in mutant IM$_{Man1A}$xIM$_{XylT1A}$ is still significantly lower
249 than in WT-Ins (Fig. 5A). This is in line with the WT-SAG and CRISPR$_{XylT1A_1}$ micropipette
250 adhesion force measurement performed in the absence of ciliobrevin D, where also
251 CRISPR$_{XylT1A_1}$ had a lower adhesion force (Fig. 4). Interestingly, addition of ciliobrevin D
252 resulted in significantly increased adhesion forces as seen for WT-SAG or WT-Ins (Fig.4 and

Fig. 5A). Taken together, these results suggested that active dynein-1b might reduce surface adhesion forces. On the other hand, it implied that IFT might be hampered via altered *N*-glycosylation as surface adhesion forces were smaller in the *N*-glycosylation mutants. Therefore, IFT velocity and gliding ability of IFT46::YFP expressing WT-Ins and IM$_{Man1A}$xIM$_{XylT1A}$ in absence of ciliobrevin D were assessed by using total internal reflection fluorescence (TIRF) microscopy. Videos of adhered cells generated by TIRF microscopy were evaluated manually with help of kymographs in Fiji software (Fig. 5B). Obtained data revealed that neither the proportion of gliding events (gliding velocity higher 0.3 µm*s^{-1}), nor gliding speed distribution was significantly diminished when comparing WT-Ins and the double mutant (Fig. 5C). Likewise, anterograde and retrograde IFT velocities were found at WT-Ins values when comparing WT-Ins and the double mutant of adherent cells (Fig. 5C), implying no significant impact of altered *N*-glycan maturation on IFT. Lastly, to rule out the possibility that ciliobrevin D might result in elevated adhesion forces due to a toxic side effect, we generated the triple mutant dynein-1b^{ts} x IM$_{Man1A}$ x IM$_{XylT1A\text{-}4\text{-}13\#}$ by crossing IM$_{Man1A}$xIM$_{XylT1A}$ with CC-4423 (Figure 5 – Supplementary Fig.1 A-C). CC-4423 is characterized by the expression of a temperature sensitive transcript of dynein-1b leading to a depletion of dynein-1b at restrictive temperatures followed by an attenuation of retrograde IFT and flagella disassembly (Engel et al., 2012). Subsequently, adhesion forces were measured via AFM at restrictive temperatures, i.e. under conditions mimicking the ciliobrevin D dependent inactivity of dynein-1b. As it cannot be excluded that flagella shortening, as induced upon temperature shift (Figure 5 – Supplementary Fig.1D), impacted flagellar adhesion forces, the triple mutant treated with 20 mM NaPPi was assessed by AFM as control. Indeed, it was found that adhesion forces differed: while control cells showed an average adhesion force of 0.48 nN, cells depleted from dynein-1b showed a significantly elevated adhesion force of 1.64 N. Importantly, NaPPi only induces flagellar shortening (Figure 5 – Supplementary Fig.1 E) but does not affect dynein-1b (Dentler

W. 2005), therefore, differences observed are directly correlated to the action of dynein-1b. It could be speculated, that the action of dynein-1b reduces flagellar adhesion forces due to its opposite direction of action with respect to the flagellar adhesion force.

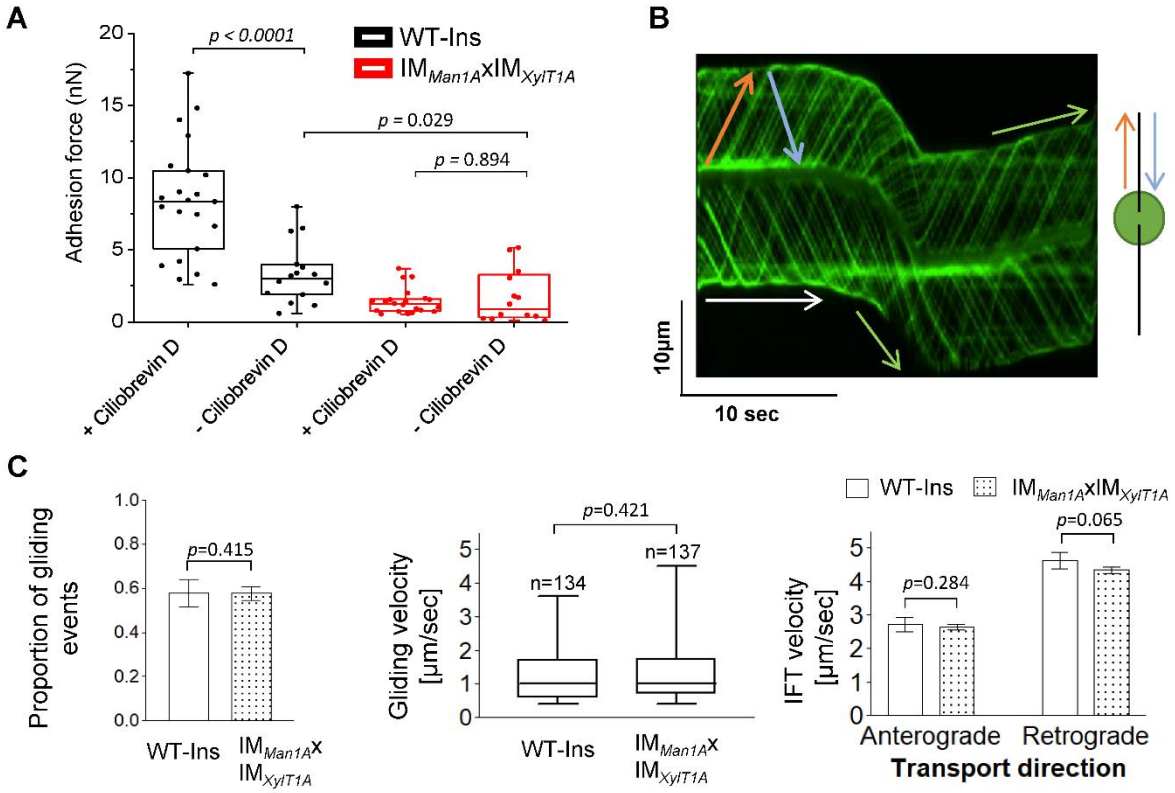

Figure 5. IFT and gliding are unaffected in IM$_{Man1A}$xIM$_{XylT1A}$

A, Adhesion forces acquired for WT-Ins and the double mutant IM$_{Man1A}$xIM$_{XylT1A}$ in the absence or presence of ciliobrevin D via AFM, respectively. Three biological replicates were performed with minimum 5 cells measured per replicate. B, Representative kymograph of the movement of IFT46::YFP in flagella of WT-Ins acquired with TIRF microscopy used to calculate the velocity of gliding and IFT. White arrow: non-gliding event (v<0.3µm*s^{-1}); green arrow: gliding event (v>0.3 µm*s^{-1}); red arrow: anterograde IFT track; blue: retrograde IFT track. C, IFT and gliding are not significantly altered in the double mutant compared to WT-Ins. Proportion of gliding events (left), gliding velocity (excluding non-gliding events; middle), IFT velocities in either direction (right). Three biological replicates were performed with 10 cells evaluated per replicate corresponding to 300 IFTs/replicates/strain in case of IFT velocity. Error bars in bar plots represent SD of three replicates. Student-t test was performed comparing mean values of replicates in regard of proportion of gliding events and IFT-velocity.

Distribution of gliding velocities was analyzed by use of Mann-Whitney U test, n represents number of gliding events measured. Gliding and IFT analysis has been performed in absence of ciliobrevin D.

Discussion

Our data revealed that the maturation of *N*-glycans has an impact on flagella mediated cell adhesion in *C. reinhardtii.* At the same time, IFT and gliding velocity were not changed due to altered *N*-glycosylation.

Microbead binding was found diminished in IM strains, implying that the flagellar surface has an altered affinity towards microbeads. In line with this, their surface adhesion forces were significantly reduced compared to WT-Ins. The AFM data were confirmed by assessing another XylT1A mutant created via CRISPR/Cas9, using micropipette force measurements. It should be noted that *N*-glycan patterns of IM$_{XylT1A}$ and CRISPR$_{XylT1A}$ were comparable and thereby strengthen the proposed role of XylT1A as core xylosyltransferase (Lucas et al., 2020; Schulze et al., 2018). Forces measured for WT strains and *N*-glycosylation mutants with AFM and micropipette force measurement confirmed that differential *N*-glycan maturation, i.e. altered *N*-glycan structures attached to mature proteins, lowers the adhesion force of flagella to a surface. These changes in adhesion forces were not accompanied by consistent drastic changes in the flagellar proteomes. For example, FMG-1B and FAP113, to date the only two known proteins involved in surface adhesion, were found in comparable amounts in WT-Ins and mutants (Fig. 1 and Figure 4 - Supplementary Fig. 2) (Bloodgood et al., 2019; Kamiya et al., 2018). Of note, also FMG-1A is localized in flagella and its abundance was unaltered between WT and mutants in vegetative cells (Figure 1 - Supplementary Fig. 4). Interestingly, gliding of mutant strains on solid surface was not affected. The current model for flagella mediated cell adhesion and subsequent gliding proposes that the extracellular part of certain glycoproteins such as FMG-

1B adheres to the surface, cytoplasmic moieties of these proteins are bound to ongoing retrograde IFT directly or indirectly upon calcium- and light dependent stimulus which is followed by an onset of gliding (Kreis et al., 2018; Shih et al., 2013). Assuming that altered *N*-glycan maturation does not impact initial protein folding in the ER (as those steps are spatially and temporally separated), our data revealed that changed *N*-glycosylation, did not alter targeting of respective glycoproteins to flagella nor the velocity of IFT. Thus, changes in surface adhesion are likely linked to *N*-glycoprotein epitopes and their direct interaction with the solid or semisolid surface. How specific *N*-glycan moieties modulate adhesion force is subject of future research, particularly considering the finding that flagella mediated adhesion of *C. reinhardtii* has been shown to be largely unaffected by different substrate surface properties (Kreis et al. 2019).

Notably, IFT and gliding were not changed between double mutant and WT-Ins (Fig. 5). The fact that altered *N*-glycosylation diminished the force of cells to adhere to surfaces but did not affect IFT, strongly suggests that adhesion to surfaces and IFT are not necessarily coupled. As discussed below, adhesion probably evolved independently of the necessity to enable cell gliding.

Moreover, it can be concluded that *N*-glycosylation does not significantly impact differences in light perception, as the adhesion forces for WT-SAG and CRISPR$_{XylT1A}$ were significantly stronger under blue than under red light (Fig. 4).

In summary, taking advantage of single-cell adhesion force measurements, our data revealed that cell adhesion was significantly impaired in *C. reinhardtii N*-glycosylation mutant strains. Our data further suggested that flagellar assembly, IFT and FMG-1B transport into flagella were not affected by altered *N*-glycosylation. Thus, we conclude that proper *N*-glycosylation of flagellar proteins is crucial for adhering *C. reinhardtii* cells onto surfaces. We further suggest

that the remaining adhesion force, although diminished in *N*-glycan mutants, is still sufficient for gliding. This suggests that the evolution of adhesion might not have been governed only by the capability of gliding but by the necessity of adhesion itself. Given the response of flagellar adhesion to blue light, it could potentially link adhesion to photo-protection which is also blue-light mediated, as adhesion might result in photoprotection via cell shading (Kreis et al., 2018; Petroutsos et al., 2016).

Material and Methods

Key Resources Table

Reagent type (species) or resource	Designation	Source or reference	Identifiers	Additional information
Strain, Strain background (*C. reinhardtii*)	WT-Ins	Lv, B. et al 2017	CC-4375	IFT46::YFP
Strain, Strain background (*C. reinhardtii*)	IM_{XylT1A}	Schulze S. et al. 2018		
Strain, Strain background (*C. reinhardtii*)	IM_{Man1a}	Schulze S. et al. 2018		
Strain, Strain background (*C. reinhardtii*)	IM_{XylT1A}x IM-$_{Man1a}$	Schulze S. et al. 2018		
Strain, Strain background (*C. reinhardtii*)	WT-SAG	AG Bäumchen, MPI Göttingen, Germany	SAG11-32b	

Strain, Strain background (*C. reinhardtii*)	CRIS-PR$_{XylT1A}$	This paper		
Strain, Strain background (*C. reinhardtii*)	dynein-1b^{ts}	Chlamycollection Engel B. et al 2012	CC-4423 dhc1b-3 mt-	
Strain, Strain background (*C. reinhardtii*)	IM$_{XylT1A}$x IM-$_{Man1a}$x dynein-1b^{ts}	This paper		
software, algorithm	Proteo-meDiscov-erer	Thermo		
software, algorithm	SugarPy	Schulz et al. 2020		
software, algorithm	Fiji, ImageJ			
Antibody	FMG1B (glycan) (mouse monoclonal)	Developmen-tal Studies Hy-bridoma Bank	AB_2722111 FMG-1B #8	
Antibody	FMG1B (peptide) (mouse monoclonal)	Developmen-tal Studies Hy-bridoma Bank	AB_2722112 FMG-1B #61	
Antibody	Anti-HRP (rabbit poly-clonal)	Abcam	ab2115	
Antibody	α-tubulin (mouse monoclonal)	SIGMA	T6199	

Antibody	ß-tubulin (mouse monoclonal)	博奥龙	BF03001	
chemical compound, drug	Ciliobrevin D		Lot3126637	Inhibitor
Other	0.75µm polystyrene microbeads	Polysciences, Inc	7309	
chemical compound, drug	Concanavalin A	Sigma		

Culture growth

Cells were grown photoheterotrophically in tris-acetate-phosphate (TAP) medium under constant illumination at 50 µmol photons*s^{-1}*cm^{-2} unless stated otherwise.

Measurement of flagellar length and flagellated cells

The cells were fixed with 0.5% Lugol's solution for 1h at room temperature. Flagellar length measurements were performed using a phase microscope (Nikon Eclipse Ti) equipped with an electron multiplying charged-coupled device. For each sample, at least 50 flagella were measured. For the measurement of flagellated cells, at least 100 cells were counted for each strain in biological triplicates.

Generation and analysis of a CRISPR/Cas9 mutant strain

Mutagenesis was performed on the WT strain SAG11-32b following the protocol described in Greiner *et al.* 2017 employing the transformation of a pre-built Cas9:guideRNA complex (Cas9 target sequence in the XylT1A gene: ACGAACACCCCAACACCAAT) simultaneously with a plasmid encoding for a paromomycin resistance via electroporation. Following selection with

paromomycin, putative mutants were screened by PCR using the primer pairs short_fw: TACAAAGAACGGGACGCAGG, short_rev: CATTGAAGCTCATCCAGACAC and long_fw: AAGGGTCACGGCACGGTATG, long_rev: CCTGAAGCACCCATGATGCACG. Genomic *XylT1A* regions of candidate strains showing not-WT like band patterns were sequenced. In total, two mutant strains differing in the DNA inserted following the Cas9 cutting site were identified (CRISPR$_{XylT1A_1}$ and CRISPR$_{XylT1A_2}$). Next, XylT1A protein levels were quantified by parallel reaction monitoring (PRM) and supernatant *N*-glycan compositions were assessed by IS-CID mass spectrometry. Additionally, flagella were isolated, separated by SDS-PAGE and, after transferred to a nitrocellulose membrane, probed with the protein backbone FMG-1B specific antibody.

Flagella isolation

Flagella isolation from cultures in the mid-log growth phase was performed as described elsewhere by the pH shock method (Witman et al., 1972). Pellets containing flagella samples were stored at -80°C until further use for immunoblotting or sample preparation for mass spectrometric measurements.

Immunoblotting

Frozen, dry flagella and whole cell samples were resuspended in lysis buffer (10mM Tris/HCl, pH=7.4, 2 % SDS, 1 mM Benzamidine and 1 mM PMSF) and subjected to sonication for 10 min. After pelleting cell debris, the protein concentration was determined using the bicinchoninic acid assay (BCA Protein Assay Kit by Thermo Scientific Pierce). Volumes corresponding to 30 µg of protein were separated by SDS-PAGE, transferred to nitrocellulose membranes and incubated with antibodies as indicated.

Lectin-affino blotting with concanavalin A and HRP

Frozen, dry whole cell samples were resuspended in lysis buffer (10mM Tris/HCl, pH=7.4, 2 % SDS, 1 mM Benzamidine and 1 mM PMSF) and subjected to sonication for 10 min. After pelleting the not-soluble cell debris, the protein concentration was determined using the bicinchoninic acid assay (BCA Protein Assay Kit by Thermo Scientific Pierce). Volumes corresponding to 50 µg of protein were separated by SDS-PAGE and transferred to nitrocellulose membrane. Membrane was incubated with ConA (1µg/ml in TBST + 1 mM $CaCl_2$ + 1 mM $MnCl_2$) for 1.5h at room temperature. Subsequently membrane was washed and incubated 1h with HRP (5µg/ml in TBST + 1 mM $CaCl_2$ + 1 mM $MnCl_2$). Excess HRP as well as Ca^{2+} and Mn^{2+} were removed by three washing steps with TBST, before affino blot was development via ECL.

Sample preparation for mass spectrometric measurements

Frozen, dry flagella and whole cell samples were treated as described in Immunoblotting. Volumes corresponding to 60 µg of protein were tryptically digested and desalted as described elsewhere (Rappsilber et al., 2007).

Mass spectrometry measurements

Tryptic peptides were reconstituted in 2 % (v/v) acetonitrile/0.1 % (v/v) formic acid in ultrapure water and separated with an Ultimate 3000 RSLCnano System (Thermo Scientific). Subsequently, the sample was loaded on a trap column (C18 PepMap 100, 300 µm x 5 mm, 5 mm particle size, 100 Å pore size; Thermo Scientific) and desalted for 5 min using 0.05 % (v/v) TFA/2 % (v/v) acetonitrile in ultrapure water with a flow rate of 10 $\mu L*min^{-1}$. Following, peptides were separated on a separation column (Acclaim PepMap100 C18, 75 mm i.D., 2 mm particle size, 100 Å pore size; Thermo Scientific) with a length of 50 cm. General mass spectrometric (MS) parameters are listed in Table 1.

For quantification of glycosyltransferases, PRM (including a target list) was employed on whole cell samples and respective spectra were analyzed with the Skyline software (Pino et al., 2017). For quantification of flagellar proteins, flagella samples were measured in biological quadruplicates in standard, not targeted, data dependent measurements. Following, peptide wise protein abundance ratios (IM/WT) were calculated with ProteomeDiscoverer™ (normalizing on a set of not membrane standing flagellar proteins) and filtered for proteins identified in at least 11 samples, for proteins having Abundance Ratio Adj. P-Value < 0.05 for at least one ratio and for proteins appearing in the flagellar proteome ChlamyFPv5(Pazour et al., 2005).

In order to assign glycopeptides, samples were measured employing In-Source collision induced dissociation (IS-CID) as described previously followed by analysis of data with Ursgal and SugarPy (Kremer et al., 2016; Oltmanns et al., 2020; Schulze et al., 2020).

Table 1. MS parameters. Relevant parameters used to acquire IS-CID and not fragmented TopN MS spectra as well as PRM data.

	TopN without IS-CID	In-Source CID HCD	Parallel reaction monitoring	
Eluent compositions	Peptide trapping: 0.05% trifluoroacetic acid (TFA) in ultrapure water (A1), 0.05% TFA in 80% acetonitrile (B1) Peptide separation: 0.1% formic acid (FA) in ultrapure water (A2), 0.1% FA in 80% acetonitrile (B2)			**LC parameters**
Trap Column	C18 PepMap 100, 300 µM x 5 mm, 5 µm particle size, 100 Å pore size; Thermo Scientific			
Peptide trapping (eluents A1+B1)	2.5% B1 at 5 µl/min for 5 min		2.5% B1 at 10 µl/min for 3 min	

Flow rate	300 nL/min		250 nL/min	
Separation Column	Acclaim PepMap C18, 75 µm x 50 cm, 2 µm particle size, 100 Å pore size; Thermo Scientific			
Gradient for peptide separation (eluents A2+B2)	2.5% B2 over 5 min, 2.5-45% B2 over 40 min, 45%-99 % B2 over 5 min 99% B2 for 20 min 99%-2.5% over 5 min 2.5% for 30 min		2.5% B2 over 5 min, 2.5-35% B2 over 105 min, 35%-99 % B2 over 5 min 99% B2 for 20 min 99%-2.5% over 5 min 2.5% for 40 min	
In-source CID	off	80 eV	off	**MS1 settings**
Use lock masses	off		on (m/z 445.12003)	
Resolution at *m/z* 200 (FWHM)	70,000			
Chromatographic peak width	15 s			
AGC target	3e6			
Maximum injection time	100 ms		50 ms	
Scan range	600-3000 m/z		350-1600 m/z	
Mass tags	off	on	off	
TopN	12		n/a	**MS2 settings**
Resolution at *m/z* 200 (FWHM)	17,500		35,000	
Isolation window	2 m/z		2 m/z (offset 0.5 m/z)	
AGC target	1e5			
Maximum injection time	120 ms			

Normalized collision energy (NCE)	30	27	
Minimum AGC target	1.25e3	n/a	
Intensity threshold	1e4	n/a	
Charge exclusion	unassigned, >5	n/a	
Dynamic exclusion	15 s	n/a	

423

424 **Microbead measurements**

425 Microbead binding- and transport assays were performed analogous to previous
426 descriptions.(Bloodgood et al., 2019) Monodisperse polystyrene microspheres (0.7 μm
427 diameter) were purchased from Polysciences, Inc. Beads were washed with deionized water for
428 three times and resuspended in NFHSM to make a store solution, which was used at 1:10
429 dilution in adhesion and motility detecting experiment.

430 To quantify the ability of bead binding, beads were added to 500 μL of cells at a density of
431 2×10^7 cells*mL^{-1}. After 5min, cells were observed with a light microscope (Olympus, U-
432 HGLGPS, 100X oil objective). A flagellum was scored as "+ bead" if beads adhered to it. The
433 percentage of flagellar binding beads was calculated as: Percentage of flagellar binding beads
434 = the number of "+ bead"/ (total number flagella scored) x 100%.

435 To obtain a kinetic measure of surface motility, cells were mixed with beads as above for 5 min
436 and randomly observed under the light microscope. Each bead adhered to a flagellum was
437 monitored for about 30 seconds. If beads moved along the flagella, we marked it as "Moved
438 bead" or it was "Adhered bead". The surface motility was calculated as: Percentage of moved
439 beads along with flagella= "Move bead" x/ ("Moved bead" + "Adhered bead") 100%.

AFM measurements

C. reinhardtii strains, grown in M1 medium under constant white illumination were grown for 65 h, were allowed to adhere to a glass slide (immersed in ethanol for overnight, subsequently rinsed with MQ water) in fresh M1 medium for 15 min. Following, cells were incubated in the presence of ciliobrevin D for 1 h (500 µL M1 supplemented with 200 µM ciliobrevin D). For AFM measurements, only adhered cells in gliding conformation having approximately similar appearance were analyzed. The MLCT-O10 AFM probe (Spring Const.: 0.03 N m^{-1}, length: 215 µm, width: 20 µm, resonant freq.: 15 kHz, Bruker) was soaked in acetone for 5 min, then subjected to UV illumination (distance to lamp: 3-5 mm) for 15 min. Then, the probe was immersed in 0.01 % poly-l-lysine for 1 h and afterwards rinsed with MQ water. Following, the probe was immersed with 2 % glutaraldehyde for 1 h and rinsed with MQ water before use. The AFM measurement was performed in Force Spectroscopy Mode in liquid at room temperature using a NanoWizard 3 AFM (JPK) equipped with a CellHesion stage (Z range: 100 µm) NanoWizard 3 head. The spring constant of the cantilever was routinely calibrated using the contact-based thermal noise method. The AFM tip, modified as described, was lowered onto the cell surface at a rate of 10 µm s^{-1} with a z scale of 25 µm. After contact, the applied force was maintained at 3 nN for 15 s. Then, the cell-attached probe was upraised at a rate of 1 µm s^{-1}. Force curves were processed with JPK SPM Data Processing (JPK). The forces and energy were determined as described in Figure 3 -Supplemental Figure 1 (Liu et al., 2011). Three biological replicates were performed with minimum 5 cells measured per replicate.

Micropipette force measurements

Cell culture growth and micropipette force measurements were performed following established recipes (Kreis et al., 2019, 2018). In brief, *C. reinhardtii* strains WT-SAG and CRISPR$_{XylT1A_1}$ grew axenically in tris-acetate-phosphate (TAP) medium (Thermo Fisher Scientific) in a Memmert IPP 100Plus incubator on a 12 h day / 12 h night cycle. The

experimental approach is based on the use of a homemade micropipette force sensor, which allows for grasping a living cell by suction (Backholm and Bäumchen, 2019). The micropipette is calibrated by measuring the deflection induced by the weight of an evaporating water droplet at tip of the pipette. The adhesion force is obtained by bringing the flagella into contact with a piece of a silicon wafer (unilateral polished, Si-Mat) cleaned by sonication in ethanol, and by measuring the micropipette deflection during iterative approach and retraction of the substrate moving at 1 $\mu m*s^{-1}$. The substrate approach consists of pushing the cell such that the micropipette is deflected by 10 µm from the cell/substrate contact position, which is then followed by a dwell period of 10 s. The substrate is then retracted by 30µm from the cell/substrate contact position at the same speed. The overall contact time between the flagella and the substrate is about 30 s. The illumination wavelength for blue and red light was 470 nm and 671 nm respectively, and realized by using narrow band pass interference filters (FWHM: 10 nm) added on top of the condenser of an inverted microscope (Olympus IX-73 and IX-83). During the adhesion force measurements, the cells were illuminated with a constant photon flux of 1019 $photons*m^{-2}* s^{-1}$ for both light conditions. For each cell, 10 adhesion force measurements were performed for each wavelength, whereby the order of red and blue light was varied randomly after 5 consecutive measurements.

In order to evaluate the influence of ciliobrevin-D on the adhesiveness, a 200 µM stock solution of ciliobrevin-D (Merck) was prepared in a 9:1 water: dimethylsulfoxide (DMSO, Purity: 99.9%, Sigma-Aldrich,) mixture. Then, 1.08 mL of this stock solution was added to 30 mL of culture to achieve a final concentration of 7 µM of ciliobrevin-D in the cell suspension. The *C. reinhardtii* suspension containing ciliobrevin-D was next incubated for 30 minutes and then centrifuged at 100 g for ten minutes, followed-up by a minimum of 30 minutes rest in the incubator. Finally, about 15 mL of the cell suspension was used to fill the liquid chamber. In parallel, a second suspension of *C. reinhardtii* cells was incubated using the same fraction of

DMSO (but without ciliobrevin-D), followed by the exact same experimental procedure to serve as a control group.

TIRF imaging

Total internal reflection microscopy (TIRF) was applied to assess intraflagellar transport and gliding behaviour of *C. reinhardtii* strains expressing YFP-coupled IFT46. Therefore, cell densities were adjusted to $1x10^5$ cells*ml^{-1}. Samples were loaded to a glass bottom microscopy chamber (µ-Slide 8 Well Glass Bottom) and refreshed every 20 min while imaging. TIRF microscopy was performed at room temperature with a Nikon Eclipse Ti and a 100x objective. IFT46::YFP was excited at 488 nm and fluorescence was recorded with an iXon Ultra EMCCD camera (Andor). For analysis, images were captured with NIS-Elements software over 30 s at 10 fps and a pixel size of 0.158 µm*$pixel^{-1}$. Images were evaluated by use of Fiji via manual evaluation of kymographs. Nett IFT velocities during gliding were calculated by subtracting corresponding gliding velocities. Three biological replicates were performed with 10 cells in gliding configuration analysed per replicate.

Confocal imaging

Cells were incubated with primary antibodies (FMG-1B #8 and #61, available at dshb.com), subsequently incubated with a fluorescently labeled secondary antibody and analyzed by confocal microscopy as described previously (Lv et al., 2017). In brief, cells were plated on 1 % poly (ethyleneimine) coated cover glass, decolorized and fixed in methanol at -20 °C for 20 min, permeated cells in PBS buffer for 1 h, and then blocked in 5 % BSA (Biosharp), 10 % normal goat serum (Dingguo) and 1 % fish gelatin (Sigma) in PBS. Incubated the samples with primary antibodies overnight, washed them, and incubated secondary antibody, washed the samples and mounted them on slides with nail polish. The slides were examined with a Leica confocal microscope (SP8). Images were acquired and processed by LAS X software

(Leica) and ImageJ software. The 488 nm laser was used YFP excitation wavelength is 510 nm, the emission wavelength is 525 nm and the exposure time is 200ms.

Mating and Tetrad analysis

The plus and minus strains was incubated in 2 mL TAP-N medium (2 x 10^7 cells/mL) under continuous light overnight for gametogenesis. 0.5 mL plus and minus gametes were mixed together and incubated for 2 h for mating. Then 0.15 mL mixture was dispersed onto mature plate (4% agar). Plate was kept in dark for 5 days, then exposed to light for 24 h. The unmated gametes were removed from the mature plate with razor blade and were killed using chloroform for 30 s. The agar contained about 30 zygotes was cut and transferred to a germination plate (1% agar). The plates were incubated in bright light till the spores were released from the zygote, then 100 μL water was added to the cut agar and was dispersed on whole plate. Single clones appeared within 3-5 days and were picked for further analysis.

Acknowledgement

The work in the laboratory of K.H. was supported by the National Nature Science Foundation of China (Grant 31671399 to Huang K). M.H. acknowledges support from the German Science Foundation (DFG, HI739/12-1). L.N.L. acknowledges funding support from the Royal Society (UF120411, URF\R\180030, RGF\EA\181061 and RGF\EA\180233) and the Biotechnology and Biological Sciences Research Council (BB/R003890/1, BB/M012441/1). China Postdoctoral Science Foundation Funded Project (Project No.: 2019M662335). A.O. and J.B. thank S. Schulze for providing SugarPy. A.G., M.K. and O.B. thank M. Lorenz and the Göttingen Algae Culture Collection (SAG) for providing the WT-SAG strain and R. Catalan for technical assistance. Thanks, Z Liang, J Huang and Professor K Jiang at Wuhan University

for sharing the TRIF microscope. Thanks D Tan and Bo Zhu and Professor L Xue at Wuhan University for sharing the AFM microscope and the technique assistance.

Author contributions:

N.X and L.H. performed light microscope imaging. A.O., J.B. and M.S. performed mass spectrometry assisted data analysis. N.X., A.O., L.H. and J.B. performed immuno blotting experiments. A.O. and S.K. performed CRISPR-Cas mutagenesis with help of P.H.. L.Z and L.L performed AFM measurements and corresponding data interpretation. A.G., M.K. and O.B. performed and analyzed micropipette force measurements. A.O., N.X., L.H., K.H. and M.H. were involved in data interpretation. A.O. wrote the manuscript with help of N.X., L.H., M.H. and K.H.

Competing Interests:

The authors declare no conflict of interests.

Materials and Correspondence:

The mass spectrometry proteomics data have been deposited to the ProteomeXchange Consortium (http://proteomecentral.proteomexchange.org) via the PRIDE partner repository with the dataset identifier PXD018353 and will be publically available upon acceptance of the manuscript (Perez-Riverol et al., 2019). During peer review, the dataset can be entered via the account reviewer44250@ebi.ac.uk and the password OLy6xQJY. For further requests, please contact K. Huang (huangky@ihb.ac.cn) or M. Hippler (mhippler@uni-muenster.de).

Literature cited

Adams BM, Oster ME, Hebert DN. 2019. Protein Quality Control in the Endoplasmic Reticulum. *Protein J* **38**:317–329. doi:10.1007/s10930-019-09831-w

Backholm M, Bäumchen O. 2019. Micropipette force sensors for in vivo force measurements on single cells and multicellular microorganisms. *Nat Protoc* **14**:594–615. doi:10.1038/s41596-018-0110-x

563 Bloodgood, R.A. (1982) Dynamic properties of the flagellar surface. Symp. Soc. Exp. Biol., 35: 353-
564 380. doi:10.1101/SQB.1982.046.01.064

565 Bloodgood RA. 2009. The Chlamydomonas Flagellar Membrane and Its Dynamic Properties
566 In: Harris EH, Stern DB, Witman GB, editors. The Chlamydomonas Sourcebook.
567 London: Academic Press. pp. 309–368. doi:10.1016/B978-0-12-370873-1.00048-4

568 Bloodgood RA. 1987. Glycoprotein dynamics in the chlamydomonas flagellar membrane.
569 *Adv Mol Cell Biol* **1**:97–130. doi:10.1016/S1569-2558(08)60358-6

570 Bloodgood RA. 1981. Flagella-dependent gliding motility in Chlamydomonas. *Protoplasma*
571 **106**:183–192. doi:10.1007/BF01275550

572 Bloodgood RA, Salomonsky NL. 1998. Microsphere attachment induces glycoprotein
573 redistribution and transmembrane signaling in the Chlamydomonas flagellum.
574 *Protoplasma* **202**:76–83. doi:10.1007/BF01280876

575 Bloodgood RA, Tetreault J, Sloboda RD. 2019. The Chlamydomonas flagellar membrane
576 glycoprotein FMG-1B is necessary for expression of force at the flagellar surface. *J Cell*
577 *Sci* **132**:1–10. doi:10.1242/jcs.233429

578 Bloodgood RA, Woodward MP, Salomonsky NL. 1986. Redistribution and shedding of
579 flagellar membrane glycoproteins visualized using an anti-carbohydrate monoclonal
580 antibody and concanavalin A. *J Cell Biol* **102**:1797–1812. doi:10.1083/jcb.102.5.1797

581 Bloodgood RA, Workman LJ. 1984. A flagellar surface glycoprotein mediating cell-substrate
582 interaction in Chlamydomonas. *Cell Motil* **4**:77–87. doi:10.1002/cm.970040202

583 Cherepanova N, Shrimal S, Gilmore R. 2016. N-linked glycosylation and homeostasis of the
584 endoplasmic reticulum. *Curr Opin Cell Biol* **41**:57–65.
585 doi:doi:10.1016/j.ceb.2016.03.021

586 Cole DG, Diener DR, Himelblau AL, Beech PL, Fuster JC, Rosenbaum JL. 1998.
587 Chlamydomonas kinesin-II-dependent intraflagellar transport (IFT): IFT particles
588 contain proteins required for ciliary assembly in Caenorhabditis elegans sensory neurons.
589 *J Cell Biol* **141**:993–1008. doi:10.1083/jcb.141.4.993

590 Collingridge P, Brownlee C, Wheeler GL. 2013. Compartmentalized calcium signaling in
591 cilia regulates intraflagellar transport. *Curr Biol* **23**:2311–2318.
592 doi:10.1016/j.cub.2013.09.059

593 Dentler W. 2005 Intraflagellar transport (IFT) during assembly and disassembly of
594 Chlamydomonas flagella. *J Cell Biol* **170**(4):649-59. doi:10.1083/jcb.200412021

595 Engel BD, Ishikawa H, Wemmer KA, Geimer S, Wakabayashi K, Hirono M, Craige B,
596 Pazour GJ, Witman GB, Kamiya R, Marshall WF 2012. The role of retrograde
597 intraflagellar transport in flagellar assembly, maintenance, and function. *J Cell Biol* **199**:
598 151-67. doi: 10.1083/jcb201206088

599 Firestone AJ, Weinger JS, Maldonado M, Barlan K, Langston LD, O'Donnell M, Gelfand VI,
600 Kapoor TM, Chen JK. 2012. Small-molecule inhibitors of the AAA+ ATPase motor
601 cytoplasmic dynein. *Nature* **484**:125–129. doi:10.1038/nature10936

602 Gardner BM, Pincus D, Gotthardt K, Gallagher CM, Walter P. 2013. Endoplasmic reticulum

603 stress sensing in the unfolded protein response. *Cold Spring Harb Perspect Biol* **5**:1–15.
604 doi:10.1101/cshperspect.a013169

605 Huangfu D, Liu A, Rakeman AS, Murcia NS, Niswander L, Anderson K V. 2003. Hedgehog
606 signalling in the mouse requires intraflagellar transport proteins. *Nature* **426**:83–87.
607 doi:10.1038/nature02061

608 Ishikawa H, Marshall WF. 2011. Ciliogenesis: Building the cell's antenna. *Nat Rev Mol Cell*
609 *Biol* **12**:222–234. doi:10.1038/nrm3085

610 Kamiya R, Shiba K, Inaba K, Kato-Minoura T. 2018. Release of Sticky Glycoproteins from
611 Chlamydomonas Flagella During Microsphere Translocation on the Surface Membrane.
612 *Zoolog Sci* **35**:299. doi:10.2108/zs180025

613 Kaulfürst-Soboll H, Rips S, Koiwa H, Kajiura H, Fujiyama K, Von Schaewen A. 2011.
614 Reduced immunogenicity of Arabidopsis hgl1 mutant N-glycans caused by altered
615 accessibility of xylose and core fucose epitopes. *J Biol Chem* **286**:22955–22964.
616 doi:10.1074/jbc.M110.196097

617 Kozminski KG, Beech PL, Rosenbaum JL. 1995. The Chlamydomonas kinesin-like protein
618 FLA10 is involved in motility associated with the flagellar membrane. *J Cell Biol*
619 **131**:1517–1527. doi:10.1083/jcb.131.6.1517

620 Kozminski KG, Johnson KA, Forscher P, Rosenbaum JL. 1993. A motility in the eukaryotic
621 flagellum unrelated to flagellar beating. *Proc Natl Acad Sci* **90**:5519 LP – 5523.
622 doi:10.1073/pnas.90.12.5519

623 Kreis CT, Grangier A, Bäumchen O. 2019. In vivo adhesion force measurements of
624 Chlamydomonas on model substrates. *Soft Matter* **15**:3027–3035.
625 doi:10.1039/c8sm02236d

626 Kreis CT, Le Blay M, Linne C, Makowski MM, Bäumchen O. 2018. Adhesion of
627 Chlamydomonas microalgae to surfaces is switchable by light. *Nat Phys* **14**:45–49.
628 doi:10.1038/NPHYS4258

629 Kremer LPM, Leufken J, Oyunchimeg P, Schulze S, Fufezan C. 2016. Ursgal, Universal
630 Python Module Combining Common Bottom-Up Proteomics Tools for Large-Scale
631 Analysis. *J Proteome Res* **15**:788–794. doi:10.1021/acs.jproteome.5b00860

632 Kukuruzinska MA, Bergh MLE, Jackson BJ. 1987. Protein glycosylation in yeast. *Antonie*
633 *Van Leeuwenhoek* **56**:915–44. doi:10.1146/annurev.bi.56.070187.004411

634 Laib JA, Marin JA, Bloodgood RA, Guilford WH. 2009. The reciprocal coordination and
635 mechanics of molecular motors in living cells. *Proc Natl Acad Sci* **106**:3190 LP – 3195.
636 doi:10.1073/pnas.0809849106

637 Lechtreck KF. 2015. IFT-Cargo Interactions and Protein Transport in Cilia. *Trends Biochem*
638 *Sci* **40**:765–778. doi:10.1016/j.tibs.2015.09.003

639 Liu L-N, Duquesne K, Oesterhelt F, Sturgis JN, Scheuring S. 2011. Forces guiding assembly
640 of light-harvesting complex 2 in native membranes. *Proc Natl Acad Sci* **108**:9455 LP –
641 9459. doi:10.1073/pnas.1004205108

642 Long H, Zhang F, Xu N, Liu G, Diener DR, Rosenbaum JL, Huang K. 2016. Comparative

643 Analysis of Ciliary Membranes and Ectosomes. *Curr Biol* **26**:3327–3335.
644 doi:10.1016/j.cub.2016.09.055

645 Lucas P-L, Mathieu-Rivet E, Chan Tchi Song P, Oltmanns A, Loutelier-Bourhis C, Plasson
646 C, Afonso C, Hippler M, Lerouge P, Mati-Baouche N, Bardor M. 2020. Multiple
647 xylosyltransferases heterogeneously xylosylate protein N -linked glycans in
648 Chlamydomonas reinhardtii. *Plant J* **102**:230–245. doi:10.1111/tpj.14620

649 Lv B, Wan L, Taschner M, Cheng X, Lorentzen E, Huang K. 2017. Intraflagellar transport
650 protein IFT52 recruits IFT46 to the basal body and flagella. *J Cell Sci* **130**:1662–1674.
651 doi:10.1242/jcs.200758

652 Mathieu-Rivet E, Scholz M, Arias C, Dardelle F, Schulze S, Le Mauff F, Teo G, Hochmal
653 AK, Blanco-Rivero A, Loutelier-Bourhis C, Kiefer-Meyer MC, Fufezan C, Burel C,
654 Lerouge P, Martinez F, Bardor M, Hippler M. 2013. Exploring the N-glycosylation
655 pathway in chlamydomonas reinhardtii unravels novel complex structures. *Mol Cell*
656 *Proteomics* **12**:3160–3183. doi:10.1074/mcp.M113.028191

657 Oltmanns A, Hoepfner L, Scholz M, Zinzius K, Schulze S, Hippler M. 2020. Novel Insights
658 Into N-Glycan Fucosylation and Core Xylosylation in C. reinhardtii. *Front Plant Sci* **10**.
659 doi:10.3389/fpls.2019.01686

660 Pazour GJ, Agrin N, Leszyk J, Witman GB. 2005. Proteomic analysis of a eukaryotic cilium.
661 *J Cell Biol* **170**:103–113. doi:10.1083/jcb.200504008

662 Pedersen LB, Rosenbaum JLBT-CT in DB. 2008. Chapter Two Intraflagellar Transport (IFT):
663 Role in Ciliary Assembly, Resorption and SignallingCiliary Function in Mammalian
664 Development. Academic Press. pp. 23–61. doi:https://doi.org/10.1016/S0070-
665 2153(08)00802-8

666 Perez-Riverol Y, Csordas A, Bai J, Bernal-Llinares M, Hewapathirana S, Kundu DJ, Inuganti
667 A, Griss J, Mayer G, Eisenacher M, Pérez E, Uszkoreit J, Pfeuffer J, Sachsenberg T,
668 Yılmaz Ş, Tiwary S, Cox J, Audain E, Walzer M, Jarnuczak AF, Ternent T, Brazma A,
669 Vizcaíno JA. 2019. The PRIDE database and related tools and resources in 2019:
670 improving support for quantification data. *Nucleic Acids Res* **47**:D442–D450.
671 doi:10.1093/nar/gky1106

672 Petroutsos D, Tokutsu R, Maruyama S, Flori S, Greiner A, Magneschi L, Cusant L, Kottke T,
673 Mittag M, Hegemann P, Finazzi G, Minagawa J. 2016. A blue-light photoreceptor
674 mediates the feedback regulation of photosynthesis. *Nature* **537**:563–566.
675 doi:10.1038/nature19358

676 Pino LK, Searle BC, Bollinger JG, Nunn B, MacLean B, MacCoss MJ. 2017. The Skyline
677 ecosystem: Informatics for quantitative mass spectrometry proteomics. *Mass Spectrom*
678 *Rev* **n/a**. doi:10.1002/mas.21540

679 Porter ME, Bower R, Knott JA, Byrd P, Dentler W. 1999. Cytoplasmic Dynein Heavy Chain
680 1b Is Required for Flagellar Assembly in Chlamydomonas. *Mol Biol Cell* **10**:693–712.
681 doi:10.1091/mbc.10.3.693

682 Rappsilber J, Mann M, Ishihama Y. 2007. Protocol for micro-purification, enrichment, pre-
683 fractionation and storage of peptides for proteomics using StageTips. *Nat Protoc*
684 **2**:1896–1906. doi:10.1038/nprot.2007.261

Roossien DH, Miller KE, Gallo G. 2015. Ciliobrevins as tools for studying dynein motor function. *Front Cell Neurosci* **9**:1–10. doi:10.3389/fncel.2015.00252

Rosenbaum JL, Witman GB. 2002. Intraflagellar transport. *Nat Rev Mol Cell Biol* **3**:813–825. doi:10.1038/nrm952

Schulze S, Oltmanns A, Fufezan C, Krägenbring J, Pohlschröder M, Hippler M. 2020. SugarPy facilitates the universal, discovery-driven analysis of intact glycopeptides. *under Rev*.

Schulze S, Oltmanns A, Machnik N, Liu G, Xu N, Jarmatz N, Scholz M, Sugimoto K, Fufezan C, Huang K, Hippler M. 2018. N-Glycoproteomic characterization of mannosidase and xylosyltransferase mutant strains of chlamydomonas reinhardtii. *Plant Physiol* **176**:1952–1964. doi:10.1104/pp.17.01450

Shih SM, Engel BD, Kocabas F, Bilyard T, Gennerich A, Marshall WF, Yildiz A. 2013. Intraflagellar transport drives flagellar surface motility. *Elife* **2013**:1–19. doi:10.7554/eLife.00744

Snell WJ, Pan J, Wang Q. 2004. Cilia and Flagella Revealed: From Flagellar Assembly in Chlamydomonas to Human Obesity Disorders. *Cell* **117**:693–697. doi:10.1016/j.cell.2004.05.019

Stanley P, Taniguchi N AM. 2017. N-glycans In: Varki A, editor. Essentials of Glycobiology. Cold Spring Harbor (NY): Cold Spring Harbor Laboratory Press. pp. 99–111. doi:10.1101/glycobiology.3e.009

Strasser R. 2016. Plant protein glycosylation. *Glycobiology* **26**:926–939. doi:10.1093/glycob/cww023

Witman GB, Carlson K, Berliner J, Rosenbaum JL. 1972. Chlamydomonas flagella: I. isolation and electrophoretic analysis of microtubules, matrix, membranes, and mastigonemes. *J Cell Biol* **54**:507–539. doi:10.1083/jcb.54.3.507

Wood CR, Huang K, Diener DR, Rosenbaum JL. 2013. The cilium secretes bioactive ectosomes. *Curr Biol* **23**:906–911. doi:10.1016/j.cub.2013.04.019

Supplementary legends

Figure 1 - Supplementary Figure 1. Flagellar length is not altered in *N*-glycosylation mutants.

a, Measurement of the flagellar length (in µm) among WT-Ins and three mutants. 50 flagella were measured in each experiment and this experiment has three biological repeats. Error bar: mean ± SD. $p>0.05$. b, Percentage of flagellated cell in WT-Ins and IM strains. The result of three biological replicates is showns. Error bar: mean ± SD. $p>0.05$.

Figure 1 - Supplementary Figure 2. *N*-Glycan structures are altered in mutants as compared to WT-Ins.

Whole cell proteins (a) and isolated flagella (b) of WT-Ins and mutants were separated on a 7% SDS-PAGE, transferred to nitrocellulose and probed with anti-HRP, which is specifically binding to β1,2-xylose and α1,3-fucose attached to the *N*-glycan core. α-tubulin, as loading controls.

Figure 1 - Supplementary Figure 3. *N*-glycosylation mutants show increased Concanavalin-A affinity

Whole cell proteins of WT-SAG, WT-Ins and mutants were separated on a 7% SDS-PAGE, transferred to nitrocellulose and probed with the lectin Concanavalin A, which binds specific N-glycan epitopes. To ensure equal protein loading membrane was stained before lectin probing with ponceau red (left).

Figure 1 - Supplementary Figure 4. Change of *N*-glycan pattern of FMG-1B in IM strains as compared to WT-Ins.

a, Diagram of the topology of FMG-1B, the major component of the glycocalyx in *C. reinhardtii*. The identified *N*-linked glycosylation sites are marked. b, Comparison of FMG-1B proteotypic *N*-glycopeptides identified by IS-CID/SugarPy in WT-Ins, IM$_{Man1A}$, IM$_{XylT1A}$ and IM$_{Man1A}$xIM$_{XylT1A}$. c, The relative peptide abundances of FMG-1A in IM$_{Man1A}$, IM$_{XylT1A}$ and IM$_{Man1A}$xIM$_{XylT1A}$ strains compared it in WT-Ins obtained by label free MS analysis.

Figure 1 - Supplementary Figure 5. Genetic crossing of original IM strains (mt+) with CC124 (mt-) to obtain mutants lacking IFT46::YFP.

a, Screening the progenies of IM$_{Man1A}$ mutants with WT-CC-124 to obtain the mutant without IFT46::YFP background, which grew in TAP plate with Paromomycin added and died in TAP plate with Hygromycin added. b, Determination of mRNA levels of *MAN1A* gene in progeny clones P14, P15 and WT-Ins. IM$_{Man1A}$ -P14 still can live in TAP plate with Paromomycin or Hygromycin. IM$_{Man1A}$ -P15 grew in TAP plate with Paromomycin and died in TAP plate added Hygromycin, which is the strain IFT46::YFP had been removed . Error bar: mean ± SD. Asterisks indicate statistically significant differences ($p < 0.01$). c, Comparison of mRNA level of *MAN1A* gene in progeny clones with CC-124. Error bar: mean+/- SD. Asterisks indicate statistically significant differences ($p < 0.01$). d, Determination of the expression of IFT46::YFP in whole cell of WT-Ins and IM$_{Man1A}$ -P15 mutant. IM$_{Man1A}$ -P15 is the offspring generated by crossing IM$_{Man1A}$ -P15 mutant (mt+) with CC124 (mt-). α-tubulin, as loading control. e, Determination of the expression of IFT46::YFP in whole cell of WT-Ins and IM$_{XylT1A}$ -P1 mutant. α-tubulin, as loading control. f, Determination of the expression of IFT46::YFP in progenies from the crossing CC124 with IM$_{Man1A}$ X IM$_{XylT1A}$. α-tubulin, as loading control.

Figure 1 - Supplementary Figure 6. The altered *N*-glycan did not change the localization FMG-1B in flagella.

(A) The mutants of $IM_{Man1A\text{-}P15}$, $IM_{XylT1A\ -P37,}$ IM_{Man1A} X $IM_{XylT1A\ -P37}$ were mixed with equal amount of WT-Ins expressing IFT46::YFP, then immune stained with an antibody against *N*-glycan epitope, there is at least one WT-Ins cell and one mutant cell in each picture. (B) The mutants of $IM_{Man1A\text{-}P15,}$ $IM_{XylT1A\ -P37,}$ IM_{Man1A} X $IM_{XylT1A\ -P37}$ were mixed with equal amount of WT-Ins expressing IFT46::YFP, then immune stained with a peptide antibody of FMG-1B, there are at least one WT-Ins cell and one mutant cell in each picture.

Figure 1 - Supplementary Figure 7. Quantitative mass spectrometry of isolated flagellar from WT-Ins and *N*-glycosylation mutants

a, Experimental procedures of flagella isolation and following analyses. b, Immunoblot of isolated flagella probed with antibodies against chloroplast marker protein (Cytf, cytochrome f) and mitochondrium marker protein (COXIIB). The absence of respective marker proteins in the flagellar fraction prove the purity of flagellar samples while ponceau staining of the same membrane indicates that similar amounts of protein were loaded. c, Proteins found significantly differential in abundance in IM strains compared to WT-Ins. Entries of proteins are given with corresponding phytozome ID protein description.

Figure 2 - Video 1. Attachment and movement of a microsphere to and along flagella.

To obtain a kinetic measure of surface motility, cells were mixed with beads as above for 5 min and randomly observed under the light microscope. Each bead adhered to a flagellum was monitored for about 30 seconds. If beads moved along the flagella, we marked it as “Moved bead” or it was “Adhered bead”. See exemplary file Figure 2 - Video 1

Figure 3 - Supplementary Figure 1. Analysis of the force and energy required to overcome the adhesion of *C. reinhardtii* flagella to the surface from AFM force curves.

The curve shows the relation of pulling force and pulling distance during AFM probe retracting. The lowest point of the curve represents the maximal adhesion force of flagella which was used in Figure 3C. The area of shaded region represents the total energy calculated by the JPK SPM Data Processing software for pulling up the cell. The average energy is calculated via dividing total energy by pulling distance as shown in the figure.

Figure 3 - Supplementary Figure 2. Detachment distance and total energy of the flagella adhesion quantified by atomic force microscopy.

A, Flagella detachment distances of WT-Ins, IM*Man1A*, IM*XylT1A* and IM*Man1A*xIM*XylT1A* were generated from force curves. B, Total energy of flagellar adhesion of WT-Ins, IM*Man1A*, IM*XylT1A* and IM*Man1A*xIM*XylT1A*. Three biological replicates were performed with

minimum 5 cells measured per replicate. *p<0.05, **p<0.01, ***p<0.001. The p values are obtained from a two-sided, two sample t-test of mean values.

Figure 4 - Supplementary Figure 1. Xylosyltransferase 1A mutant generated via CRISPR/Cas9 supports findings in IM*XylT1A*.

a, Schematic representation of the XylT1A gene including the site targeted by CIRSPR/Cas9. b, Parallel reaction monitoring was employed to prove the knock out of XylT1A on proteomic level in two mutants generated by CRISPR/Cas9. c, Comparison of *N*-glycan patterns between the XylT1A mutant strains in different genetic backgrounds (IM strain and CRISPR-Cas generated mutants) considering comparable *N*-glycosites. d, Detailed comparison of the *XylT1A* strains in different genetic background looking specifically at Pent (left), dHex (middle) and *N*-glycan length (number of Hex+MeHex, right).

Figure 4 - Supplementary Figure 2. Immunoblot proving the presence of FMG-1B in flagella of CRISPR*XylT1A.1* and CRISPR*XylT1A.2*

30 µg of protein per sample were separated by SDS-PAGE and transferred to a nitrocellulose membrane in biological quadruplicates. a, Ponceau staining of the membrane reveals equal loading between different strains and differential composition of different sample types. b, On one hand, the FMG-1B protein backbone specific antibody proves a correct targeting of FMG-1B to flagella in the mutants despite altered N-glycosylation. On the other, the application of antibodies specifically binding to a chloroplast (Cytf, cytochrome f) marker protein as well as to the ATPase beta subunit (mitochondrial and chloroplast) proves the purity of flagellar samples analyzed.

Figure 4 - Supplementary Figure 3. Study of the effect of DMSO on the flagella adhesion forces using micropipette force microscopy

Micropipette force measurements of the same cells were performed for WT-SAG under blue and red light in the (+) presence or (-) absence of DMSO. The concentration of DMSO corresponds to the one used in the experiments with Ciliobrevin-D. Mean values of 10 measurements per cell are depicted, statistical analysis was performed on mean values. The p-values obtained a from Kolmogorov-Smirnov test are respectively (from top to bottom): (n.s.) p=0.9556, (*) p=0.0415.

Figure 5 Supplementary Figure 1. Adhesion force increases in temperature sensitive dhc1-b mutant at restrictive temperature.

(A) The unique inserted cassette of *AphVIII* in *MAN1A* gene was identified in the double mutant and the progenies of the cross between the IM*Man1A* IM*XylT1A* with dynein-1b^{ts} using PCR. (B) Identification of the point mutation of DHC1b^{ts} in the progenies of the cross between the IM-*Man1A* IM*XylT1A* and dynein-1b^{ts}. (C) Identification of the unique inserted fragment of *XylT1A* gene in the progenies of the cross between theIM*Man1A* IM*XylT1A* and dynein-1b^{ts} using PCR. (D)

The shortening of flagella occurs only when triple mutant was incubated at restrictive temperature. Three biological replicates were performed with 50 flagella evaluated per replicate. Error bars show SEM of three replicates. (E) The flagella were shortening when triple mutant was treated with 20 mM Nappi. Three biological replicates were performed with 50 flagella evaluated per replicate. Error bars show SEM of three replicates. (F) The distribution of adhesive force when triple mutant was incubated at restrictive temperature (- no functional DHC1b) or treated with 20 mM NaPPi (+ with functional DHC1b). Three biological replicates were performed with at least 4 cells evaluated per replicate. T-test was used for statistical analysis. Asterisks indicate statistically differences (*$p < 0.01$). (G) The total energy of pulled up cell from the solid surface. Three biological replicates were performed with at least 4 cells evaluated per replicate. T-test was used for statistical analysis. Asterisks indicate statistically differences (*$p < 0.1$).

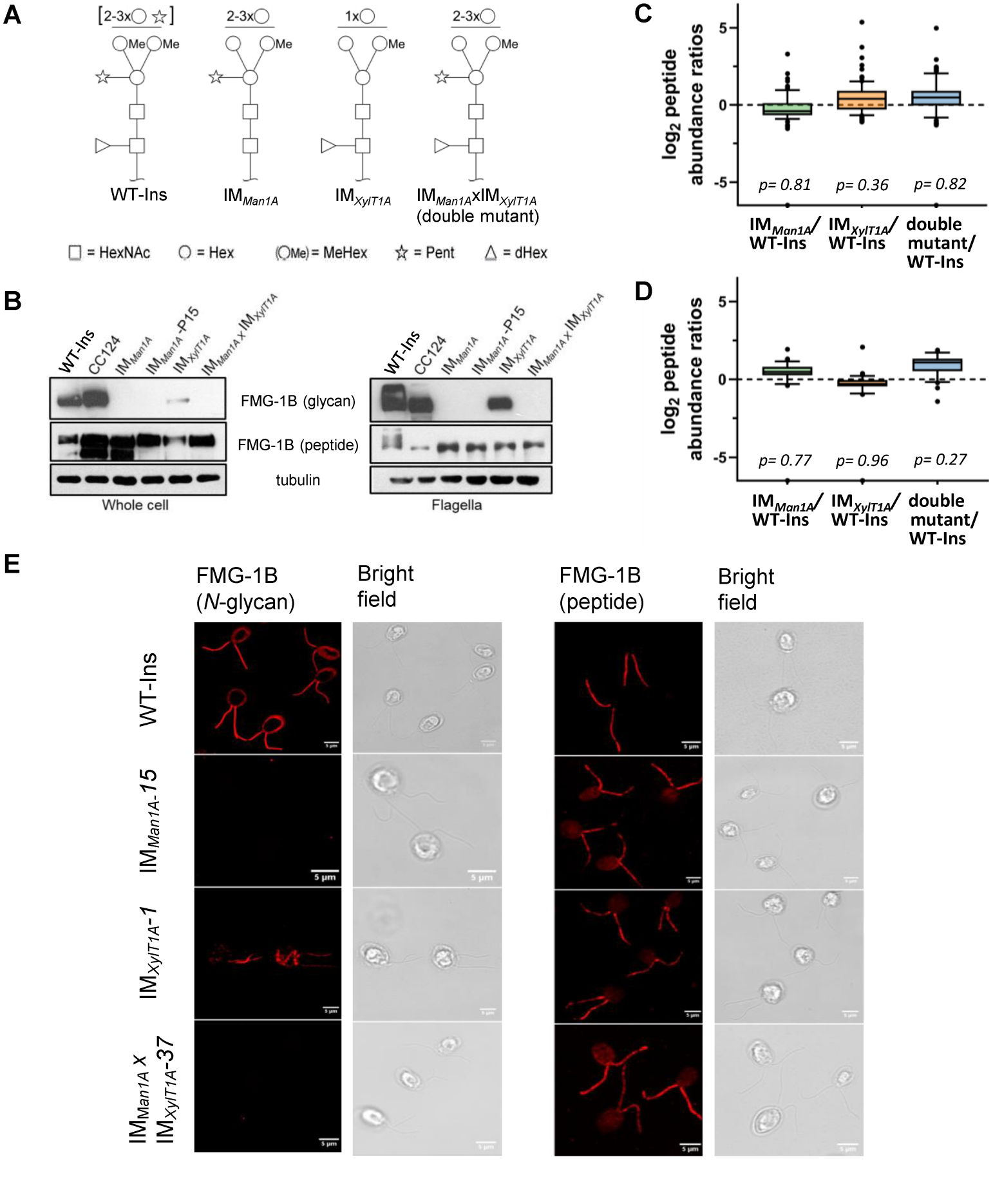
A
[2-3x ☆]
2-3x
1x
2-3x
Me
WT-Ins
IM Man1A
IM XylT1A
IM Man1A x IM XylT1A
(double mutant)
= HexNAc
= Hex
= MeHex
= Pent
= dHex
B
WT-Ins
CC124
IM Man1A
IM Man1A -P15
IM XylT1A
IM Man1A x IM XylT1A
FMG-1B (glycan)
FMG-1B (peptide)
tubulin
Whole cell
Flagella
C
log2 peptide abundance ratios
5
0
-5
p= 0.81
p= 0.36
p= 0.82
IM Man1A/ WT-Ins
IM XylT1A/ WT-Ins
double mutant/ WT-Ins
D
log2 peptide abundance ratios
5
0
-5
p= 0.77
p= 0.96
p= 0.27
IM Man1A/ WT-Ins
IM XylT1A/ WT-Ins
double mutant/ WT-Ins
E
FMG-1B (N-glycan)
Bright field
FMG-1B (peptide)
Bright field
WT-Ins
IM Man1A-15
IM XylT1A-1
IM Man1A x IM XylT1A-37
5 µm

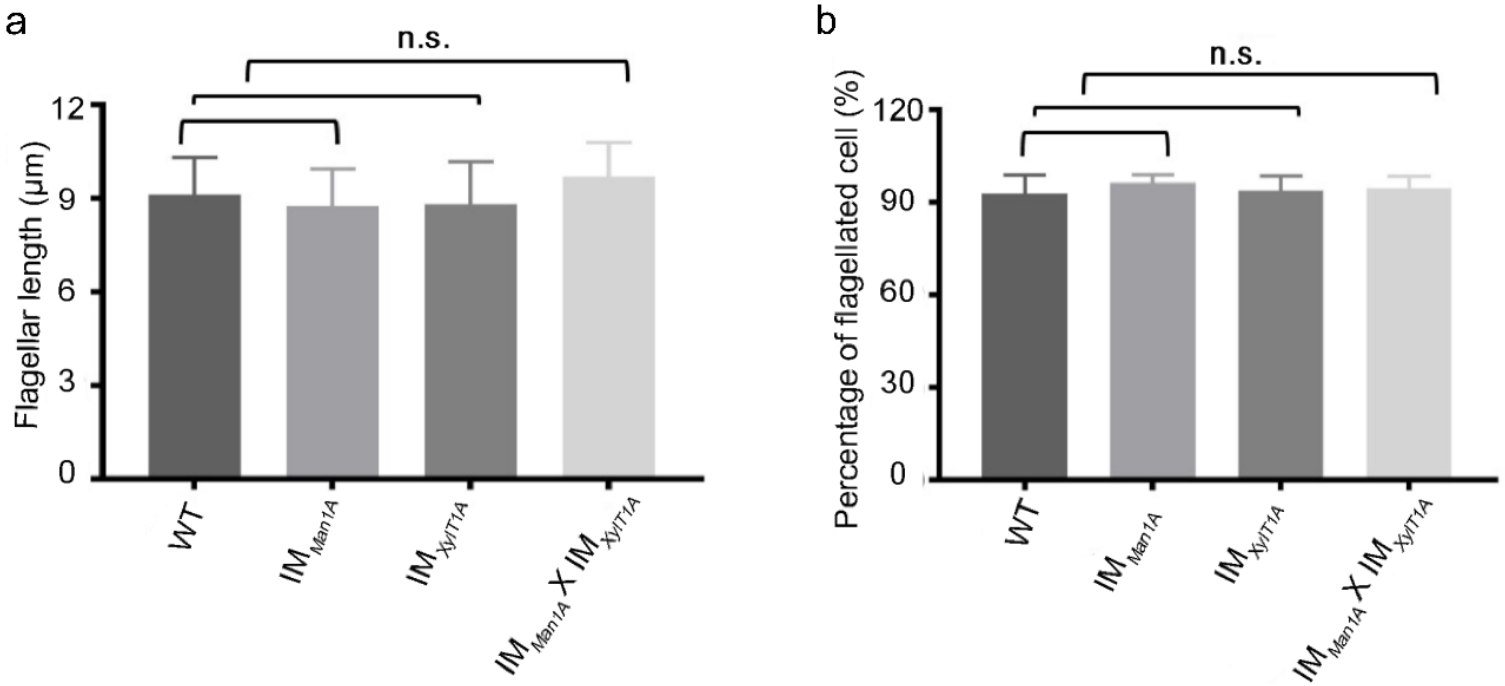
a
n.s.
Flagellar length (μm)
12
9
6
3
0
WT
IM Man1A
IM XylT1A
IM Man1A X IM XylT1A
b
n.s.
Percentage of flagellated cell (%)
120
90
60
30
0
WT
IM Man1A
IM XylT1A
IM Man1A X IM XylT1A

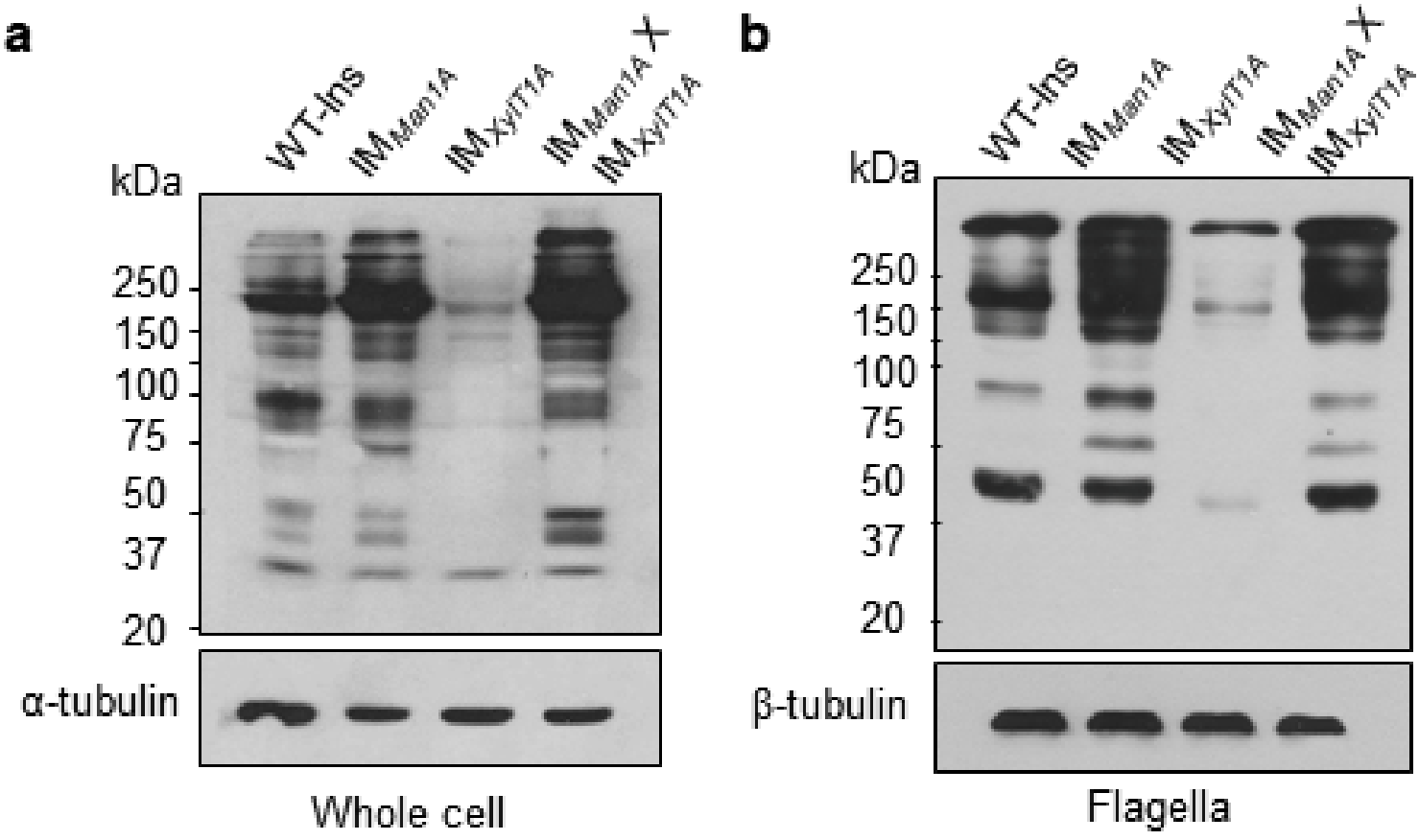
a
WT-ins
IMMan1A
IMXylT1A
IMMan1A X
IMXylT1A
kDa
250
150
100
75
50
37
20
α-tubulin
Whole cell
b
WT-ins
IMMan1A
IMXylT1A
IMMan1A X
IMXylT1A
kDa
250
150
100
75
50
37
20
β-tubulin
Flagella

a

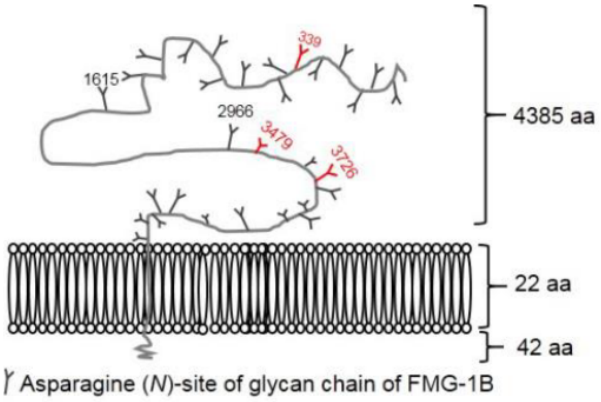

b

N-glycosylated peptide of FMG-1B	*N*-glycan chain	Strain
ADCDAVFVFSGAGNTTK	Hex(4)HexNAc(2)MeHex(2)Pent(2)dHex(1)	WT
	Hex(5)HexNAc(2)MeHex(1)Pent(1)dHex(0)	IM_{Man1A}
	Hex(6)HexNAc(2)MeHex(1)Pent(1)dHex(0)	
	Hex(7)HexNAc(2)MeHex(0)Pent(1)dHex(0)	
	Hex(6)HexNAc(2)MeHex(0)Pent(1)dHex(0)	IM_{XylT1A}
	Hex(6)HexNAc(2)MeHex(0)Pent(0)dHex(0)	
	Hex(5)HexNAc(2)MeHex(0)Pent(0)dHex(0)	
	Hex(7)HexNAc(2)MeHex(0)Pent(1)dHex(0)	
	Hex(5)HexNAc(2)MeHex(1)Pent(0)dHex(0)	
	Hex(5)HexNAc(2)MeHex(1)Pent(1)dHex(0)	IM_{Man1A} x IM_{XylT1A}
	Hex(6)HexNAc(2)MeHex(0)Pent(0)dHex(1)	
	Hex(7)HexNAc(2)MeHex(0)Pent(1)dHex(0)	
	Hex(6)HexNAc(2)MeHex(0)Pent(1)dHex(0)	
LLSAGNFSAGDTVNIKPEQAELR	Hex(4)HexNAc(2)MeHex(2)Pent(2)dHex(1)	WT
	Hex(3)HexNAc(2)MeHex(3)Pent(2)dHex(1)	
	Hex(6)HexNAc(2)MeHex(0)Pent(1)dHex(0)	IM_{Man1A}
	Hex(4)HexNAc(2)MeHex(1)Pent(1)dHex(0)	
	Hex(5)HexNAc(2)MeHex(0)Pent(2)dHex(0)	
	Hex(6)HexNAc(2)MeHex(0)Pent(2)dHex(0)	
	Hex(3)HexNAc(2)MeHex(1)Pent(1)dHex(0)	IM_{XylT1A}
	Hex(3)HexNAc(2)MeHex(1)Pent(0)dHex(1)	
	Hex(6)HexNAc(2)MeHex(0)Pent(1)dHex(1)	
	Hex(2)HexNAc(2)MeHex(1)Pent(1)dHex(0)	
	Hex(5)HexNAc(2)MeHex(0)Pent(1)dHex(0)	
	Hex(5)HexNAc(2)MeHex(1)Pent(1)dHex(1)	
	Hex(4)HexNAc(2)MeHex(0)Pent(0)dHex(1)	
	Hex(4)HexNAc(2)MeHex(1)Pent(1)dHex(0)	
	Hex(5)HexNAc(2)MeHex(1)Pent(1)dHex(0)	IM_{Man1A} x IM_{XylT1A}
	Hex(5)HexNAc(2)MeHex(0)Pent(2)dHex(0)	
	Hex(6)HexNAc(2)MeHex(0)Pent(1)dHex(0)	
SVIIAAANSTAAK	Hex(3)HexNAc(2)MeHex(3)Pent(2)dHex(1)	WT
	Hex(2)HexNAc(2)MeHex(5)Pent(2)dHex(1)	
	Hex(7)HexNAc(2)MeHex(0)Pent(1)dHex(0)	IM_{Man1A}
	Hex(3)HexNAc(2)MeHex(1)Pent(0)dHex(1)	IM_{XylT1A}
	Hex(7)HexNAc(2)MeHex(0)Pent(1)dHex(0)	IM_{Man1A} x IM_{XylT1A}

c

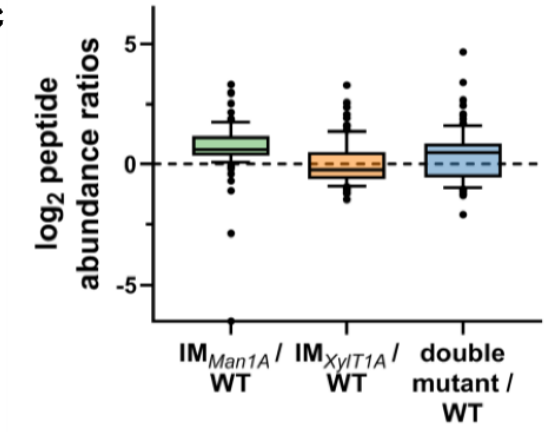

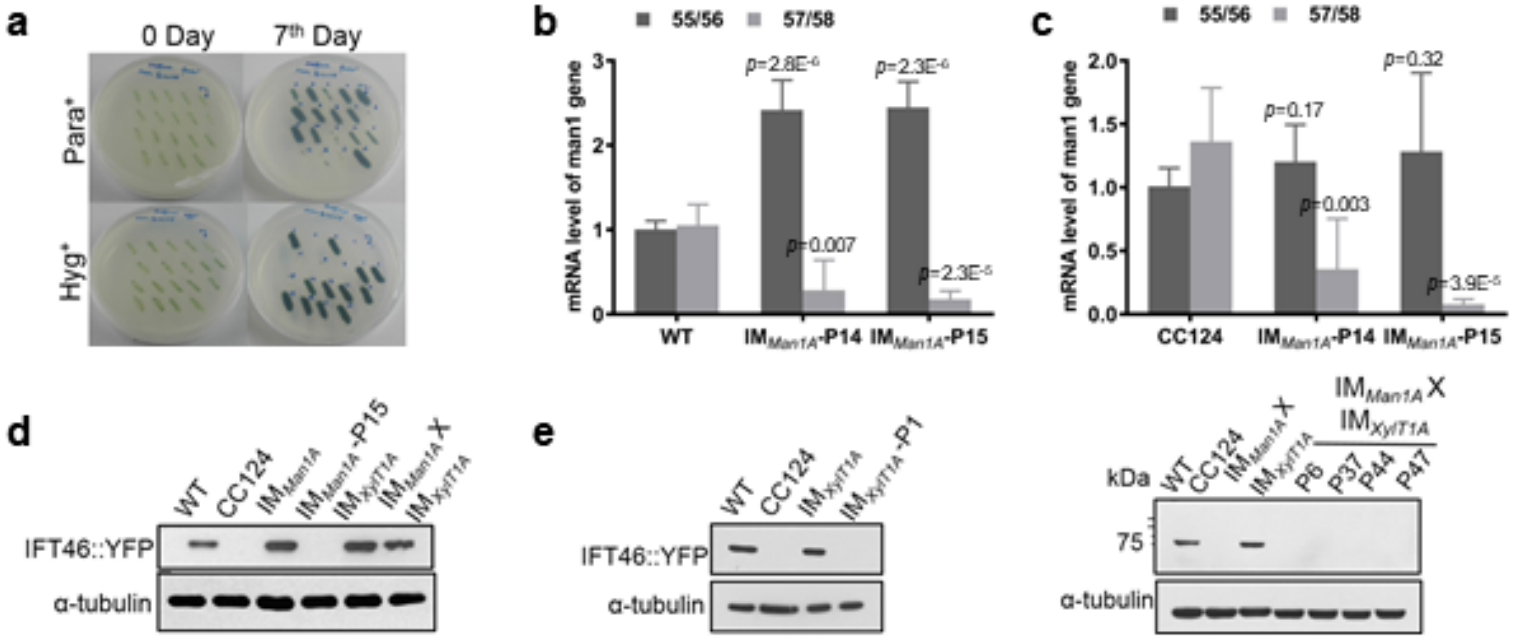
a
0 Day
7th Day
Para+
Hyg+
b
55/56
57/58
mRNA level of man1 gene
p=2.8E-6
p=2.3E-6
p=0.007
p=2.3E-5
WT
IMMan1A-P14
IMMan1A-P15
c
55/56
57/58
mRNA level of man1 gene
p=0.17
p=0.32
p=0.003
p=3.9E-5
CC124
IMMan1A-P14
IMMan1A-P15
d
WT
CC124
IMMan1A
IMMan1A -P15
IMXylT1A
IMMan1A X
IMXylT1A
IFT46::YFP
α-tubulin
e
WT
CC124
IMXylT1A
IMXylT1A -P1
IFT46::YFP
α-tubulin
IMMan1A X
IMXylT1A
kDa
WT
CC124
IMMan1A
IMXylT1A
P6
P37
P44
P47
75
α-tubulin

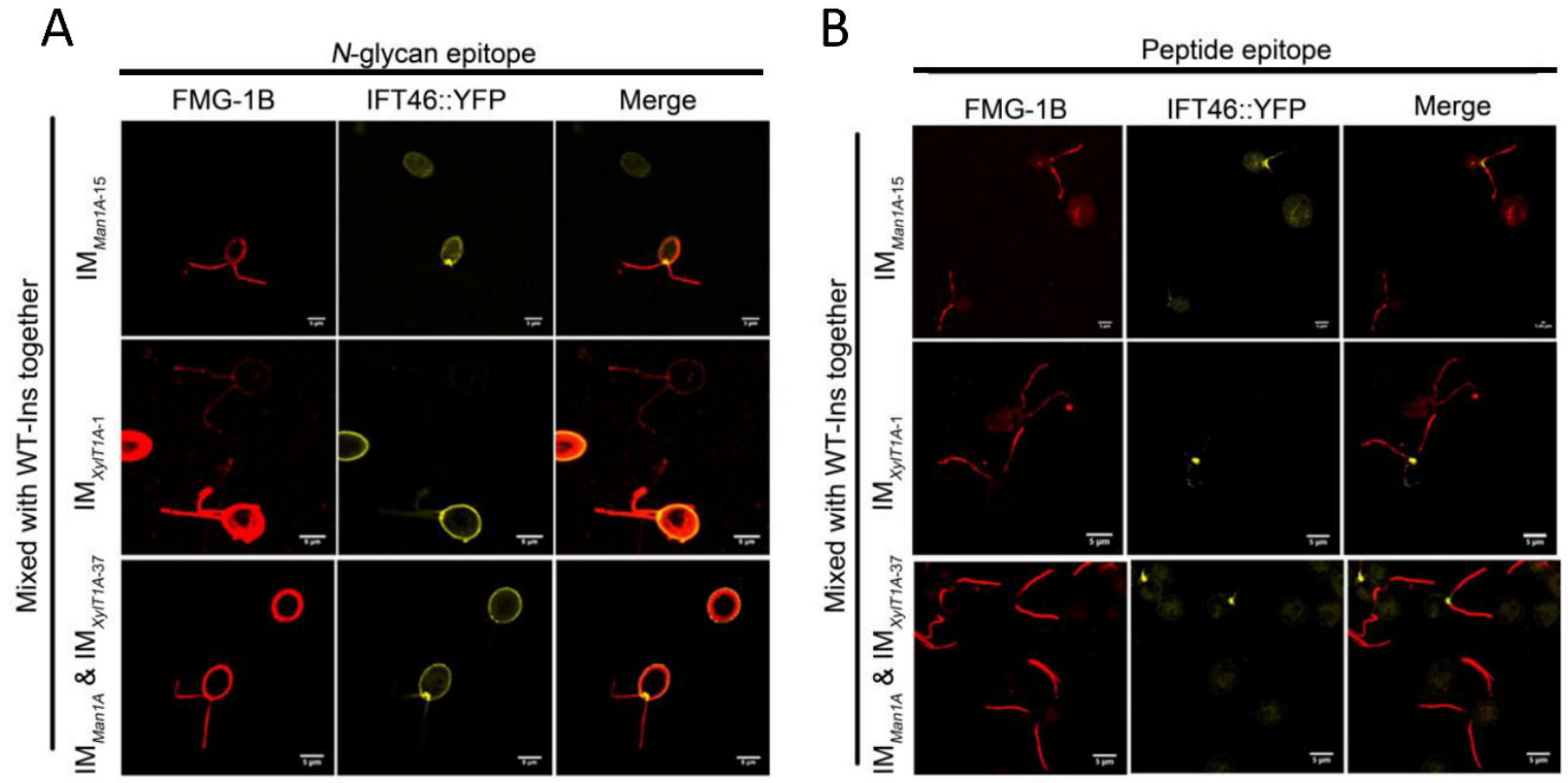
A
N-glycan epitope
FMG-1B
IFT46::YFP
Merge
Mixed with WT-Ins together
IMMan1A-15
IMXylT1A-1
IMMan1A & IMXylT1A-37
B
Peptide epitope
FMG-1B
IFT46::YFP
Merge
Mixed with WT-Ins together
IMMan1A-15
IMXylT1A-1
IMMan1A & IMXylT1A-37

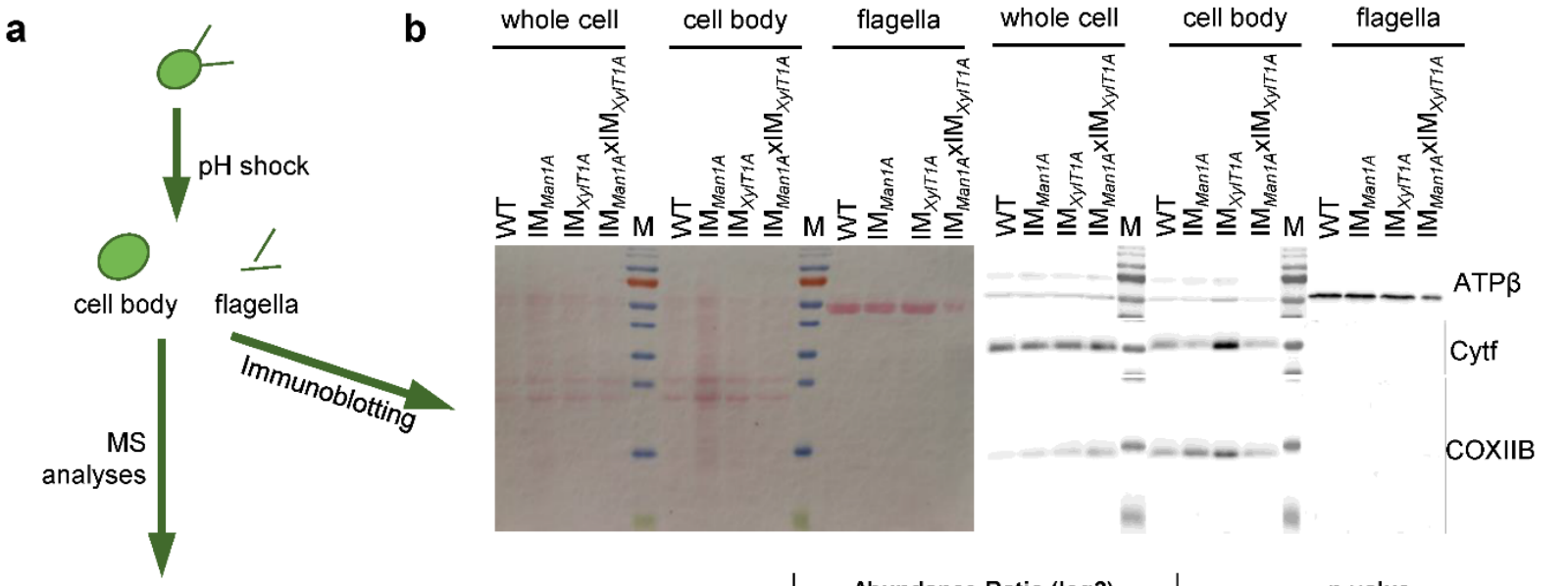

c

Accession number	Description	Abundance Ratio (log2) IM(Man1)/(WT)	IM(XylT1A)/WT	double mutant/WT	p-value IM(Man1)/(WT)	IM(XylT1A)/WT	double mutant/WT
Cre08.g366101.t1.1	Cre08.g366101.t1.1	-1.08	-0.72	0.26	*	0.37	0.96
Cre02.g147750.t1.2	Flagellar Associated Protein; FAP209	-0.12	0.80	0.28	0.86	*	1.00
Cre09.g397660.t1.1	Cre09.g397660.t1.1	-0.10	-1.11	1.15	0.87	*	0.75
Cre17.g718900.t1.2	Flagellar Associated Protein; FAP88	0.02	1.32	0.95	0.93	*	0.72
Cre17.g712900.t1.1	Cre17.g712900.t1.1	0.03	-1.51	-0.12	0.95	*	0.90
Cre08.g358564.t1.1	FAP344	0.08	-0.07	1.74	0.99	0.99	*
Cre02.g077800.t1.2	FAP310	0.09	-1.48	1.46	0.99	*	*
Cre01.g010900.t1.2	Glyceraldehyde-3-Phosphate Dehydrogenase	0.10	-0.78	1.91	1.00	0.29	*
Cre06.g278222.t1.1	{RCK1} Receptor of activated protein kinase C	0.13	-0.46	2.37	0.98	0.83	*
Cre03.g156250.t1.2	FAP186	0.18	-0.30	1.56	0.94	0.98	*
Cre01.g027000.t1.2	Ribosomal protein L11	0.19	-1.08	2.07	0.99	*	0.09
Cre09.g396100.t1.2	Cell wall protein pherophorin-C15	0.19	-0.92	1.67	0.95	0.13	*
Cre14.g620600.t1.2	Cell wall protein pherophorin-C2; FAP202	0.21	-1.76	2.31	0.93	*	*
Cre12.g543500.t1.2	Cre12.g543500.t1.2; FAP364	0.27	-0.29	1.33	0.91	0.99	*
Cre01.g047550.t1.2	Small Rab-related GTPase	0.28	-1.27	1.05	0.92	*	0.86
Cre12.g492600.t1.2	Fasciclin-like protein; FAP346	0.28	-1.15	-0.05	0.89	*	0.92
Cre16.g693600.t1.2	Hydroxyproline-rich cell wall protein; FAP 137	0.29	-0.37	2.51	0.93	0.92	*
Cre06.g290950.t1.2	Ribosomal protein S5	0.32	-0.95	2.58	0.93	0.10	*
Cre17.g701200.t2.1	Ribosomal protein L14	0.34	-0.29	1.80	0.87	0.99	*
Cre14.g632350.t1.1	Flagellar Associated Protein; FAP 138	0.34	0.18	1.44	0.87	0.85	*
Cre02.g081050.t1.2	Flagellar Associated Protein; FAP24	0.35	-1.14	0.21	0.87	*	0.99
Cre02.g101350.t1.2	Ribosomal protein L10a	0.56	-0.19	2.32	0.69	0.99	*
Cre02.g090050.t1.1	Flagellar Associated Protein; FAP170	0.57	-0.18	1.65	0.69	0.99	*
Cre05.g234550.t1.2	Fructose-1,6-bisphosphate aldolase	0.60	-0.47	1.76	0.62	0.82	*
Cre06.g308250.t1.2	Ribosomal protein S4	0.62	-0.41	2.31	0.67	0.89	*
Cre12.g520500.t1.1	Acidic ribosomal protein P0	0.63	-0.65	2.59	0.54	0.51	*
Cre12.g522600.t1.2	mitochondrial cytochrome c	0.64	-0.37	2.46	0.67	0.92	*
Cre01.g066917.t1.1	Chlorophyll a/b binding protein of LHCII	0.70	-0.51	1.87	0.43	0.77	*
Cre09.g398900.t1.1	Vegetative cell wall protein gp1	0.70	-0.41	1.62	0.41	0.88	*
Cre10.g459250.t1.2	Ribosomal protein L35a	0.73	-0.30	3.42	0.71	0.98	*
Cre05.g238650.t1.1	Cell wall protein pherophorin-C5	0.76	-1.11	3.22	0.61	*	*
Cre07.g356850.t1.1	Cre07.g356850.t1.1	0.76	0.94	0.79	0.71	*	0.96
Cre02.g120100.t1.2	Ribulose-1,5-bisphosphate carboxylase	0.78	-0.79	2.60	0.31	0.27	*
Cre12.g483950.t1.2	NAD-dependent malate dehydrogenase, mitochondrial	0.79	-1.09	3.04	0.43	*	*
Cre16.g693700.t1.2	Ubiquitin-conjugating enzyme E2	0.80	-1.28	-0.19	0.25	*	0.86
Cre12.g548400.t1.2	Light-harvesting protein of photosystem II	0.82	-0.66	2.00	0.23	0.48	*
Cre07.g347100.t1.2	Cre07.g347100.t1.2	0.86	-0.26	1.35	0.17	0.99	*
Cre06.g258800.t1.1	FAP3	0.89	-0.07	1.43	0.15	0.99	*
Cre12.g550850.t1.2	Oxygen-evolving enhancer protein 2 of photosystem II	1.47	-0.22	2.06	*	0.99	*
Cre08.g372450.t1.2	Oxygen evolving enhancer protein 3	1.48	-0.62	2.16	*	0.58	*
Cre12.g500550.t1.2	Cre12.g500550.t1.2	1.56	0.22	1.99	*	0.78	0.40

A

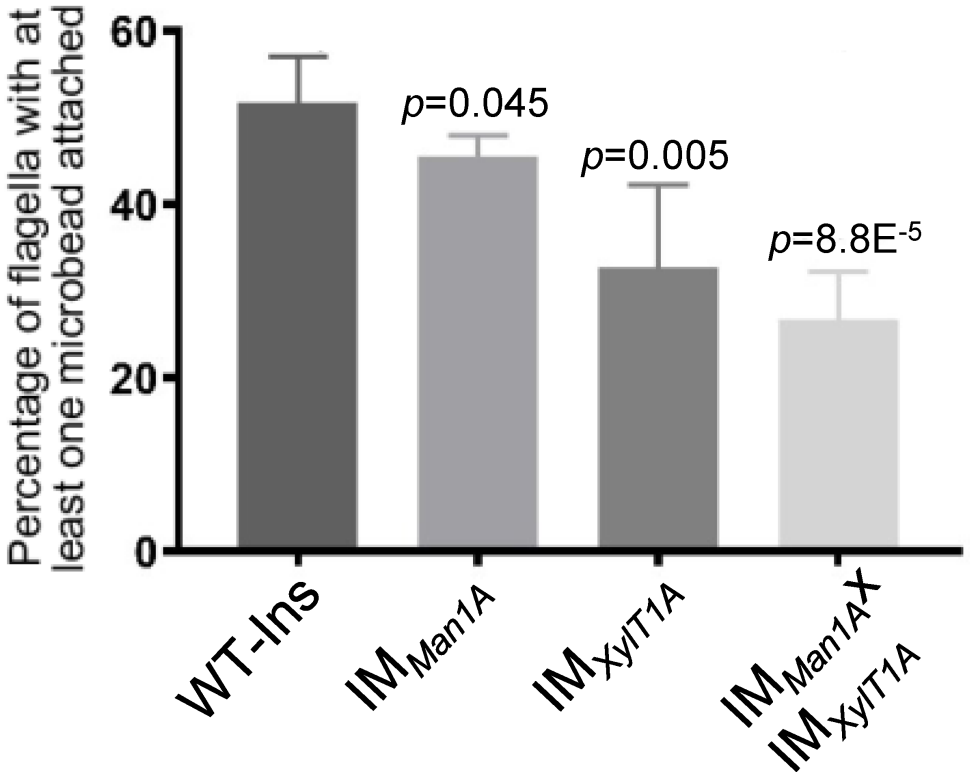
Percentage of flagella with at least one microbead attached
60
40
20
0
p=0.045
p=0.005
p=8.8E-5
WT-Ins
IM Man1A
IM XylT1A
IM Man1A X IM XylT1A

B

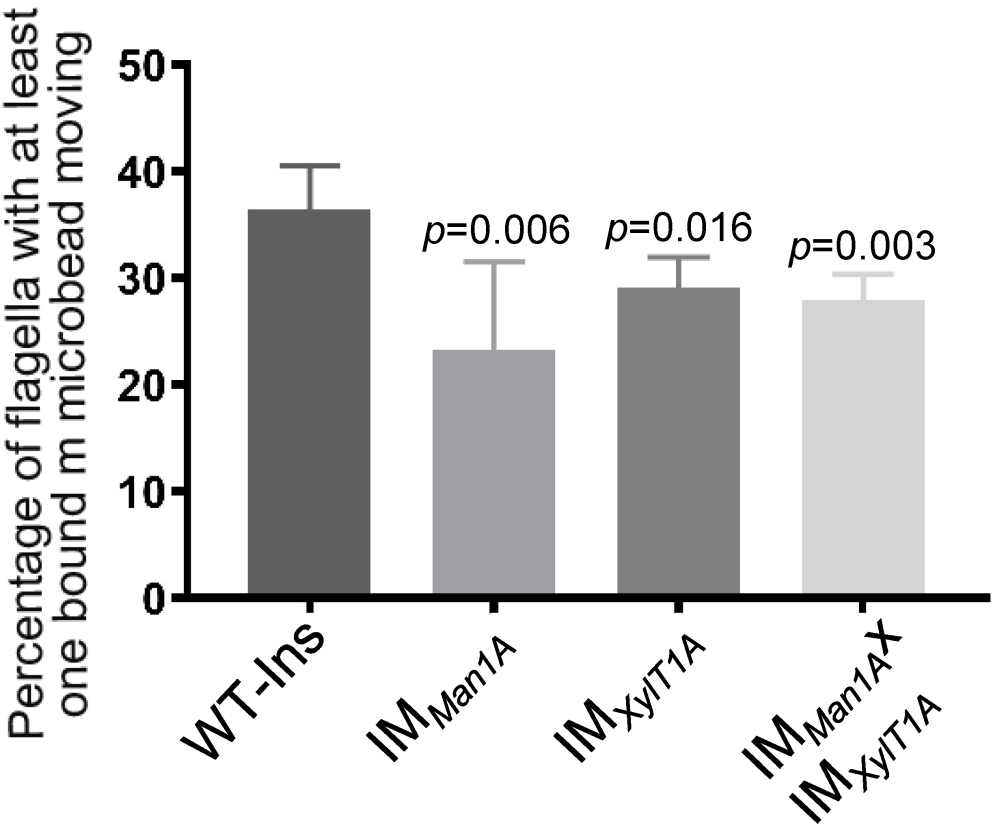
Percentage of flagella with at least one bound m microbead moving
50
40
30
20
10
0
p=0.006
p=0.016
p=0.003
WT-Ins
IM Man1A
IM XylT1A
IM Man1A X IM XylT1A

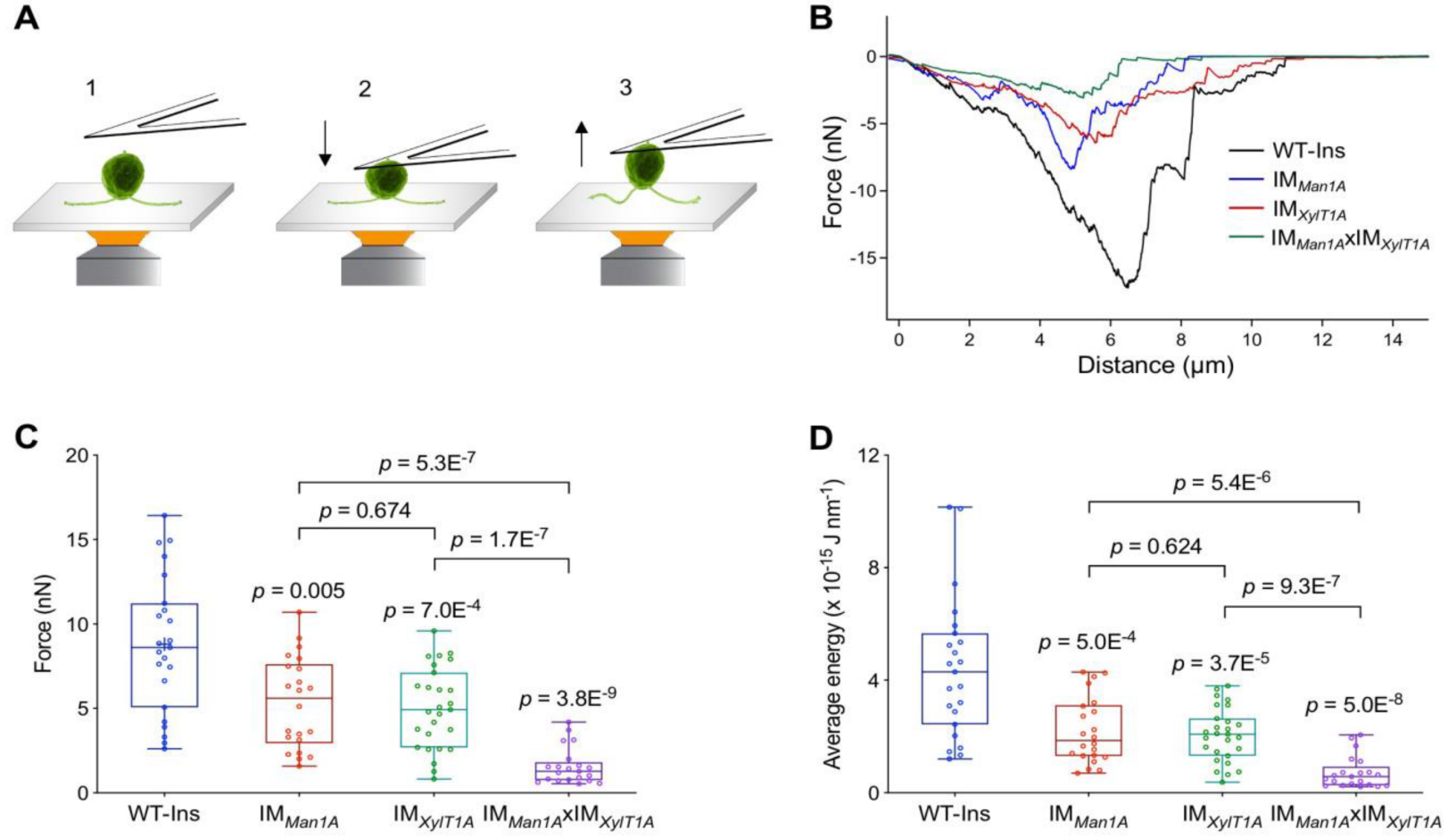
A
1
2
3
B
Force (nN)
Distance (µm)
WT-Ins
IM$_{Man1A}$
IM$_{XylT1A}$
IM$_{Man1A}$xIM$_{XylT1A}$
C
Force (nN)
p = 5.3E-7
p = 0.674
p = 1.7E-7
p = 0.005
p = 7.0E-4
p = 3.8E-9
WT-Ins
IM$_{Man1A}$
IM$_{XylT1A}$
IM$_{Man1A}$xIM$_{XylT1A}$
D
Average energy (x 10^{-15} J nm^{-1})
p = 5.4E-6
p = 0.624
p = 9.3E-7
p = 5.0E-4
p = 3.7E-5
p = 5.0E-8
WT-Ins
IM$_{Man1A}$
IM$_{XylT1A}$
IM$_{Man1A}$xIM$_{XylT1A}$

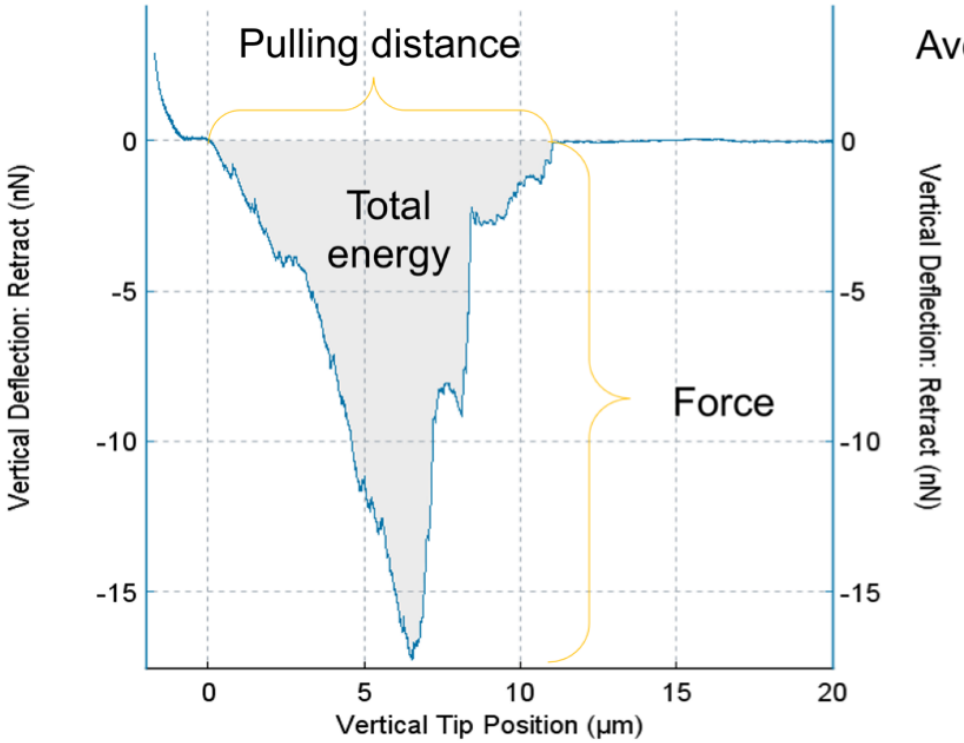

$$\text{Average energy} = \frac{\text{Total energy}}{\text{Pulling distance}}$$

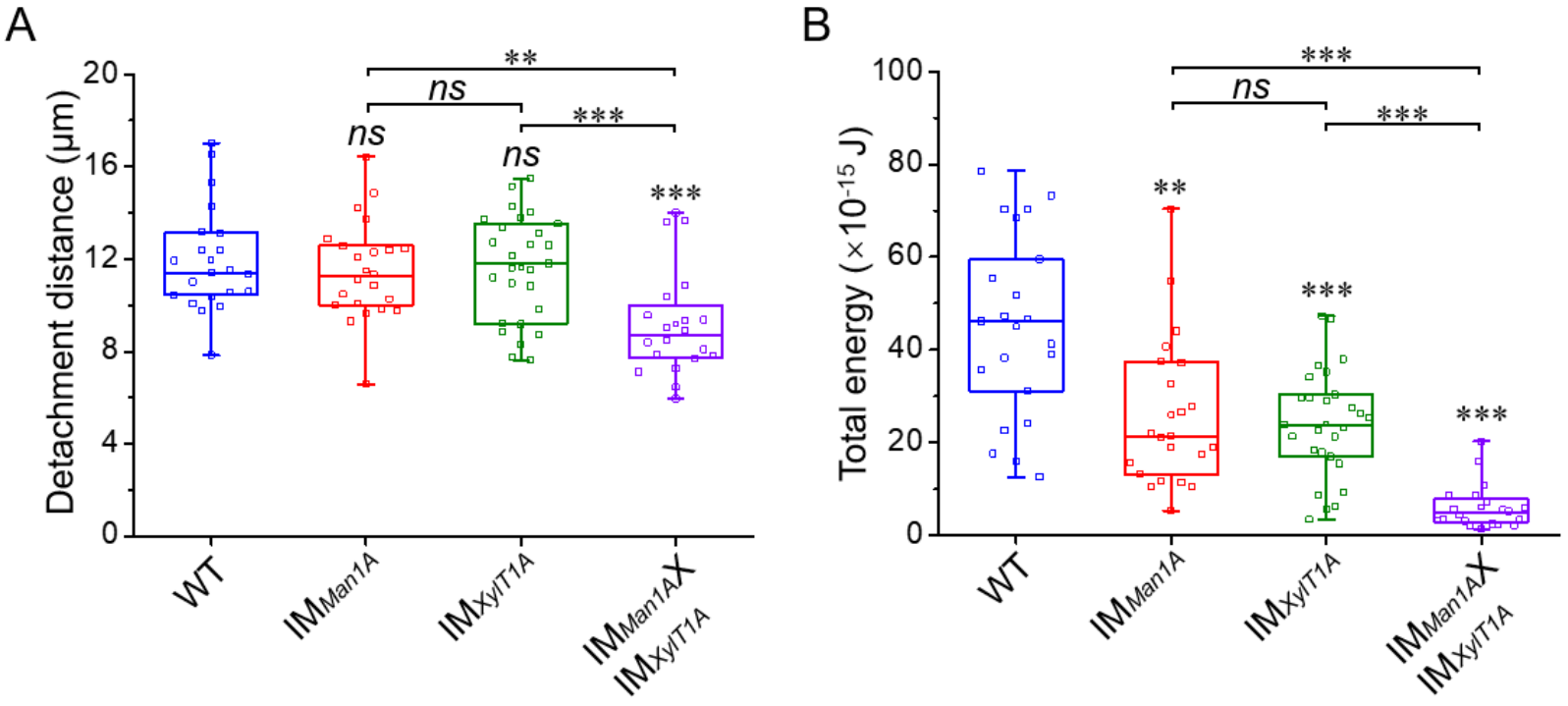
A
Detachment distance (μm)
0
4
8
12
16
20
**
ns
ns
ns
***
***
WT
IMMan1A
IMXylT1A
IMMan1AXIMXylT1A
B
Total energy (×10-15 J)
0
20
40
60
80
100
***
ns
ns
**
***
***
WT
IMMan1A
IMXylT1A
IMMan1AXIMXylT1A

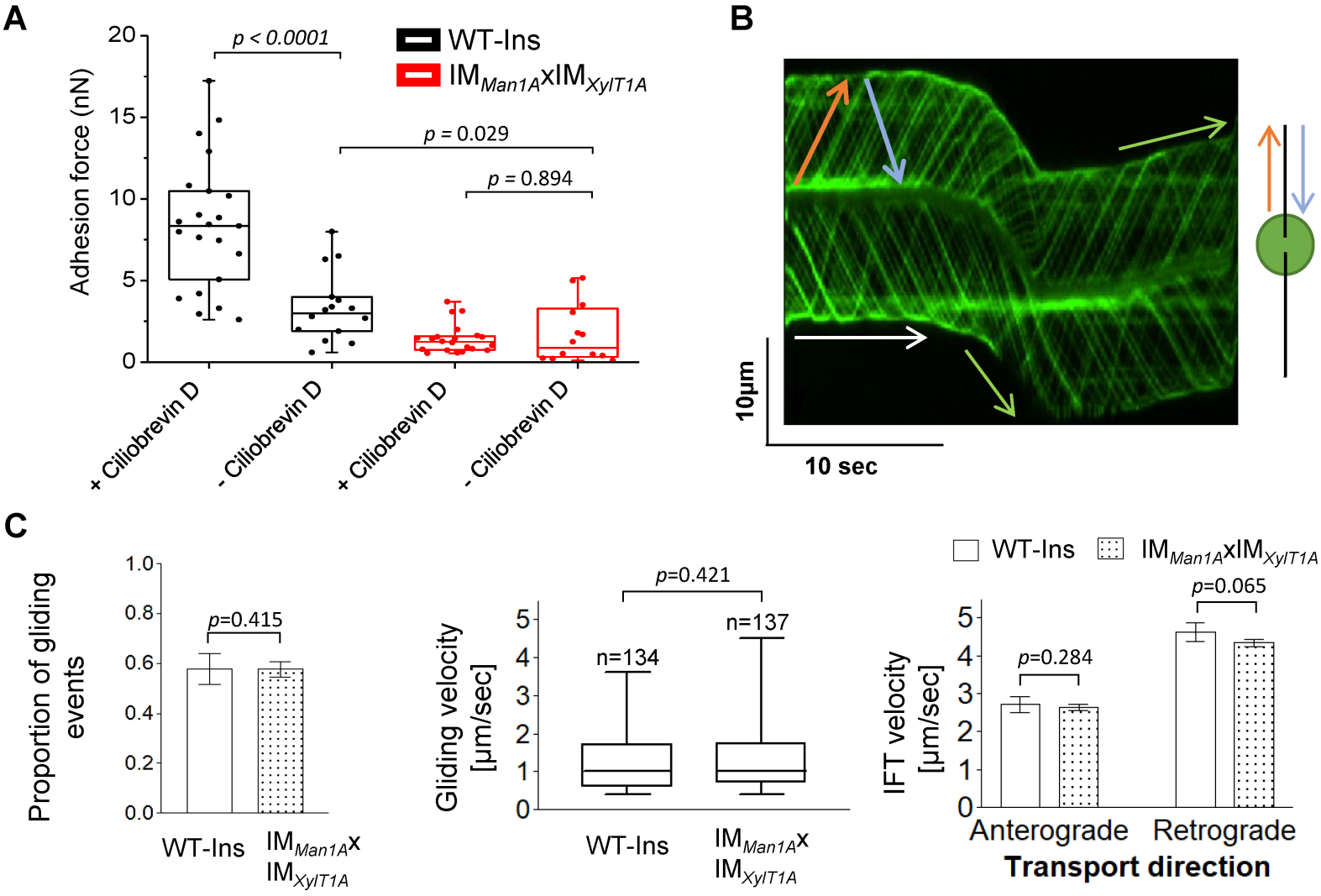
A
Adhesion force (nN)
20
15
10
5
0
p < 0.0001
p = 0.029
p = 0.894
WT-Ins
IMMan1AxIMXylT1A
+ Ciliobrevin D
- Ciliobrevin D
+ Ciliobrevin D
- Ciliobrevin D
B
10µm
10 sec
C
Proportion of gliding events
1.0
0.8
0.6
0.4
0.2
0.0
p=0.415
WT-Ins
IMMan1Ax IMXylT1A
Gliding velocity [µm/sec]
5
4
3
2
1
0
p=0.421
n=134
n=137
WT-Ins
IMMan1Ax IMXylT1A
WT-Ins
IMMan1AxIMXylT1A
IFT velocity [µm/sec]
p=0.284
p=0.065
Anterograde
Retrograde
Transport direction

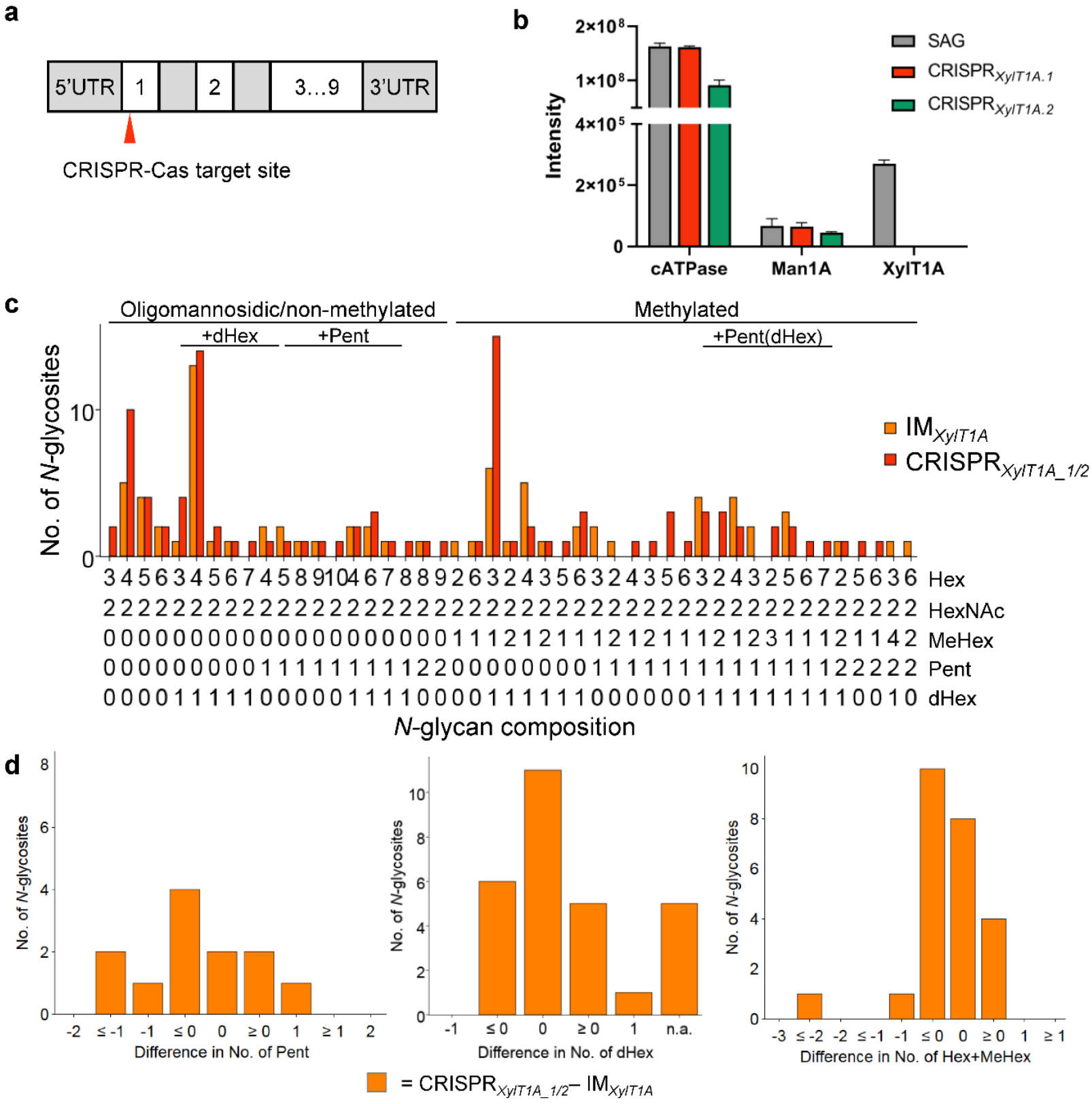
a
5'UTR
1
2
3…9
3'UTR
CRISPR-Cas target site
b
Intensity
2×10^8
1×10^8
4×10^5
2×10^5
0
SAG
CRISPR XylT1A.1
CRISPR XylT1A.2
cATPase
Man1A
XylT1A
c
Oligomannosidic/non-methylated
Methylated
+dHex
+Pent
+Pent(dHex)
No. of N-glycosites
IM XylT1A
CRISPR XylT1A_1/2
Hex
HexNAc
MeHex
Pent
dHex
N-glycan composition
d
No. of N-glycosites
Difference in No. of Pent
Difference in No. of dHex
Difference in No. of Hex+MeHex
= CRISPR XylT1A_1/2 – IM XylT1A

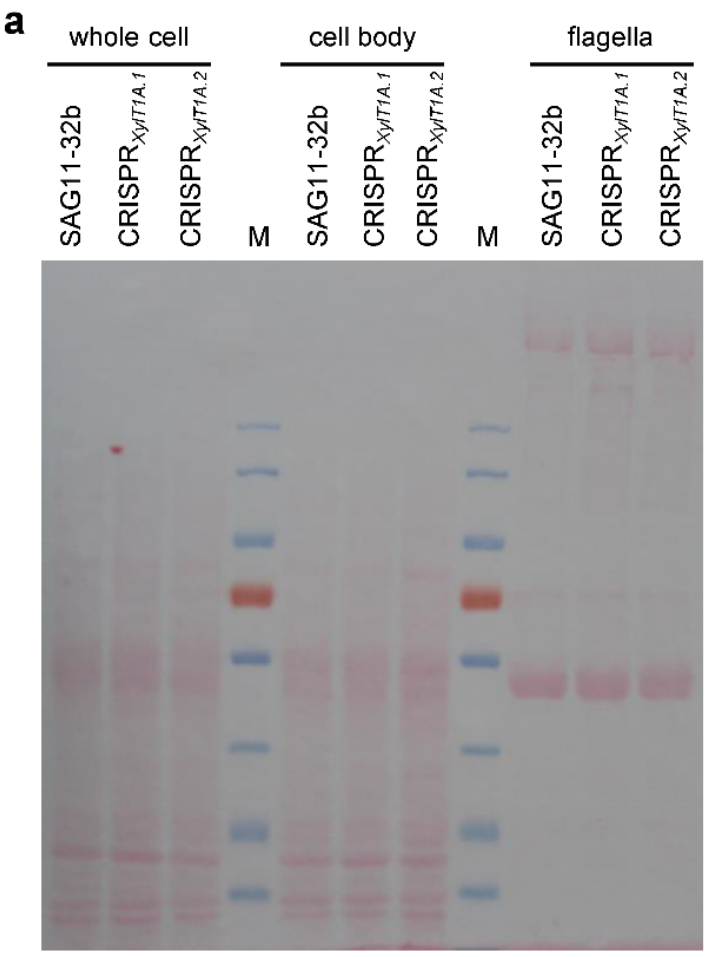
a
whole cell
cell body
flagella
SAG11-32b
CRISPR$_{XylT1A.1}$
CRISPR$_{XylT1A.2}$
M
SAG11-32b
CRISPR$_{XylT1A.1}$
CRISPR$_{XylT1A.2}$
M
SAG11-32b
CRISPR$_{XylT1A.1}$
CRISPR$_{XylT1A.2}$

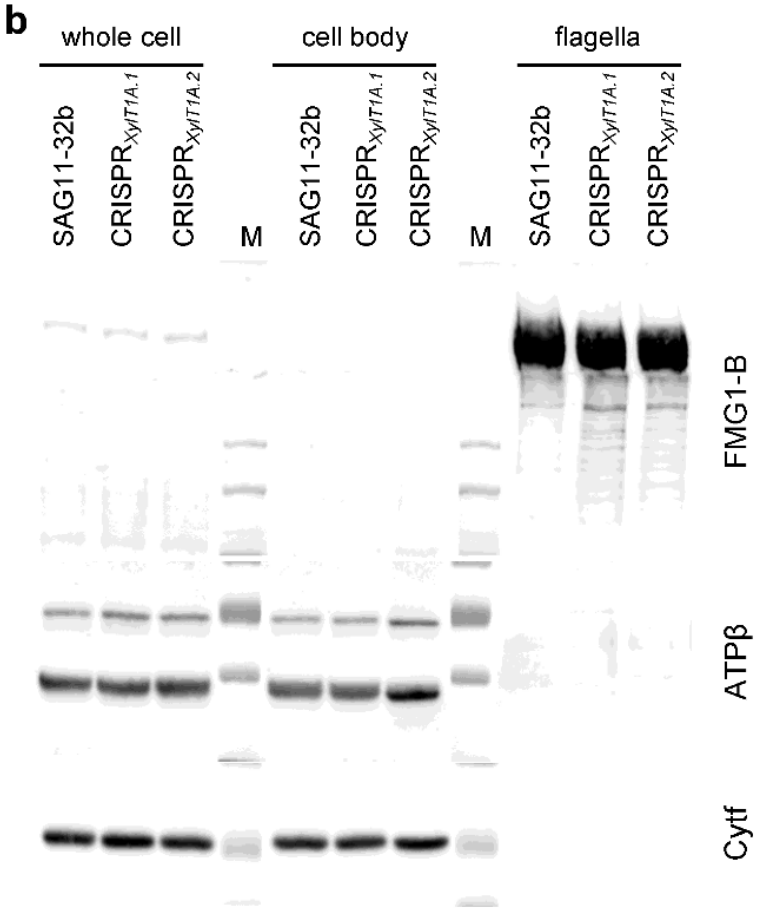
b
whole cell
cell body
flagella
SAG11-32b
CRISPR$_{XylT1A.1}$
CRISPR$_{XylT1A.2}$
M
SAG11-32b
CRISPR$_{XylT1A.1}$
CRISPR$_{XylT1A.2}$
M
SAG11-32b
CRISPR$_{XylT1A.1}$
CRISPR$_{XylT1A.2}$
FMG1-B
ATPβ
Cytf

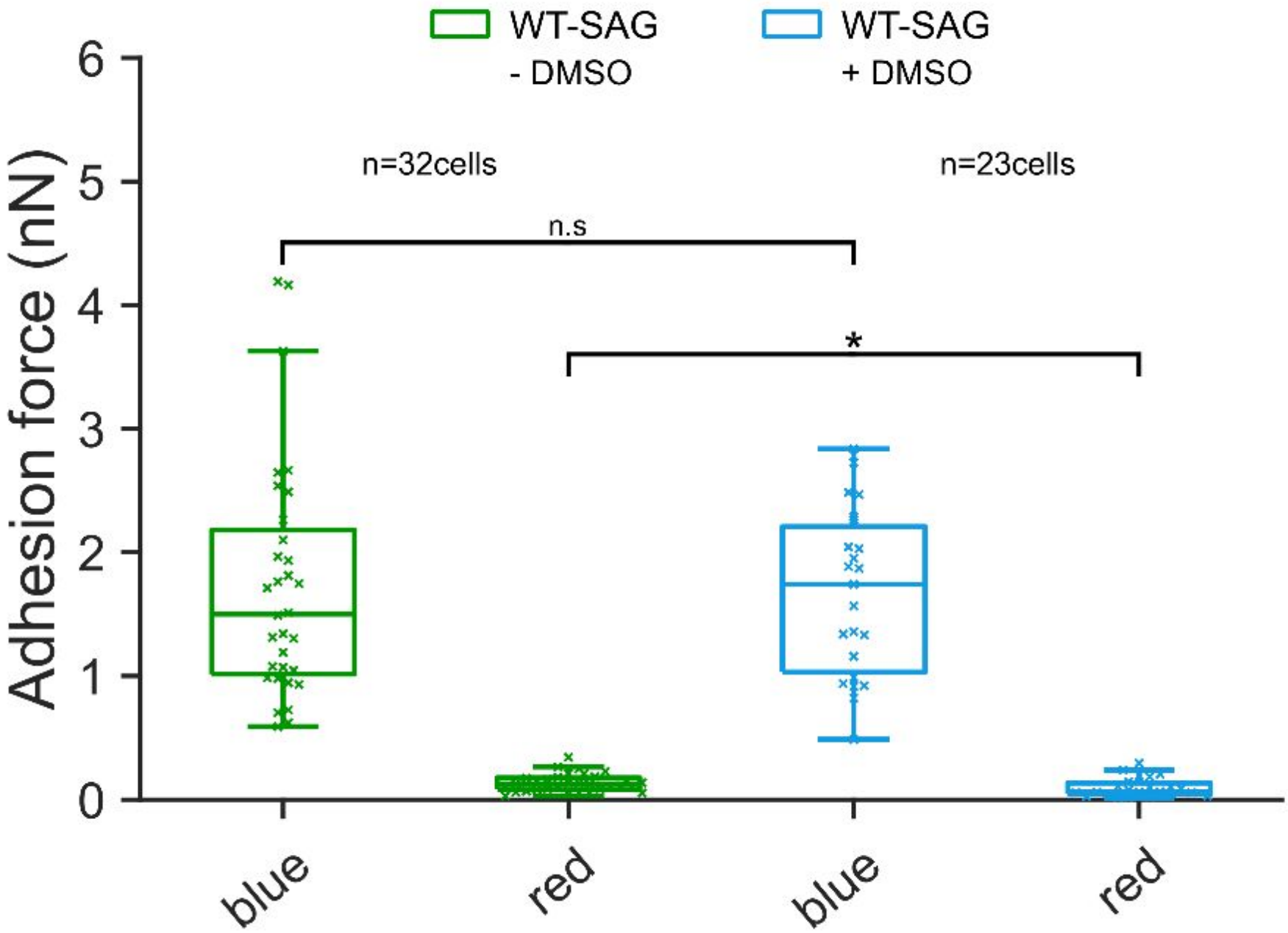
WT-SAG
- DMSO
WT-SAG
+ DMSO
n=32cells
n=23cells
n.s
*
Adhesion force (nN)
0
1
2
3
4
5
6
blue
red
blue
red

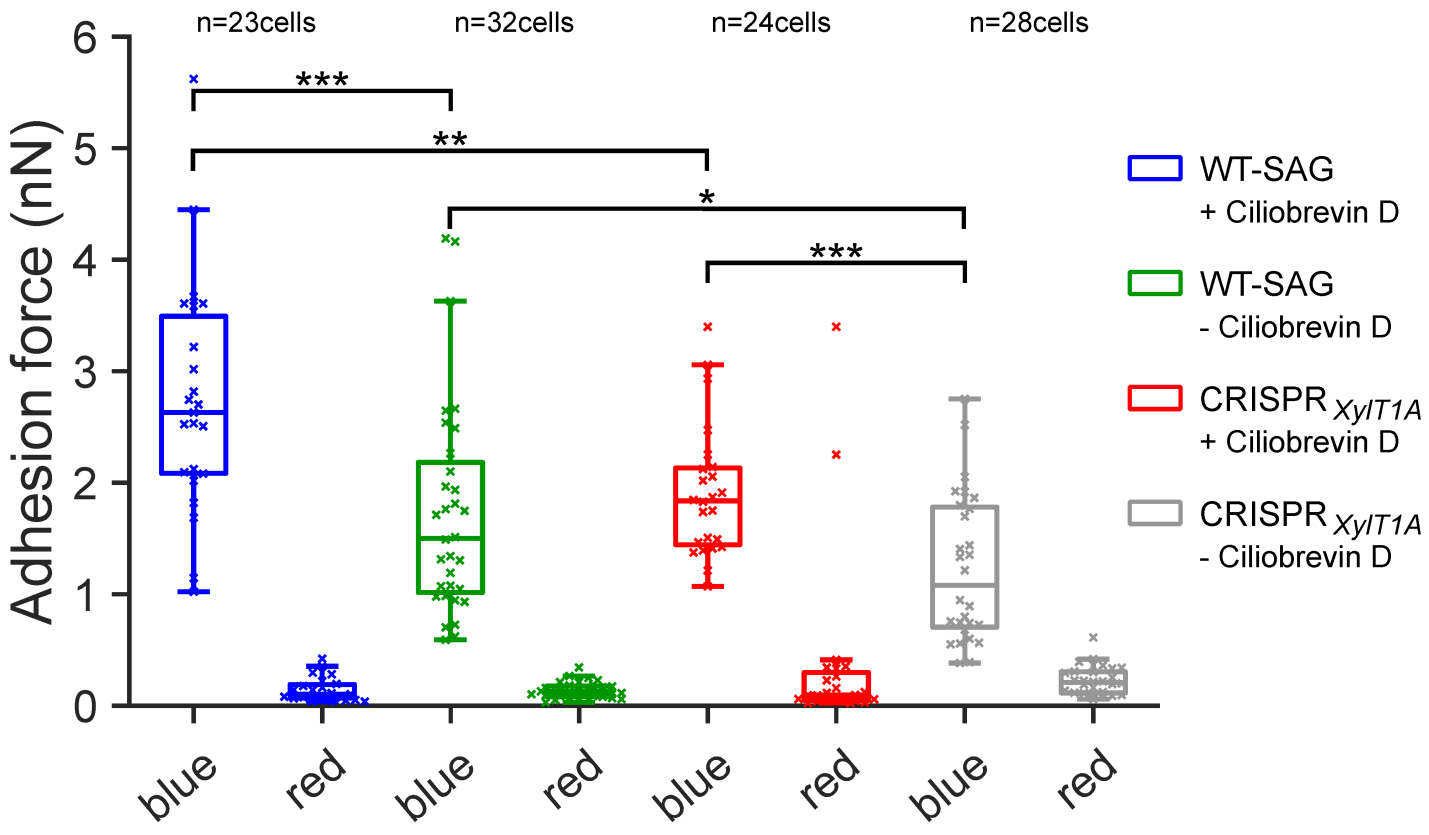
n=23cells
n=32cells
n=24cells
n=28cells
Adhesion force (nN)
0
1
2
3
4
5
6
***
**
*
***
blue
red
blue
red
blue
red
blue
red
WT-SAG
+ Ciliobrevin D
WT-SAG
- Ciliobrevin D
CRISPR XylT1A
+ Ciliobrevin D
CRISPR XylT1A
- Ciliobrevin D

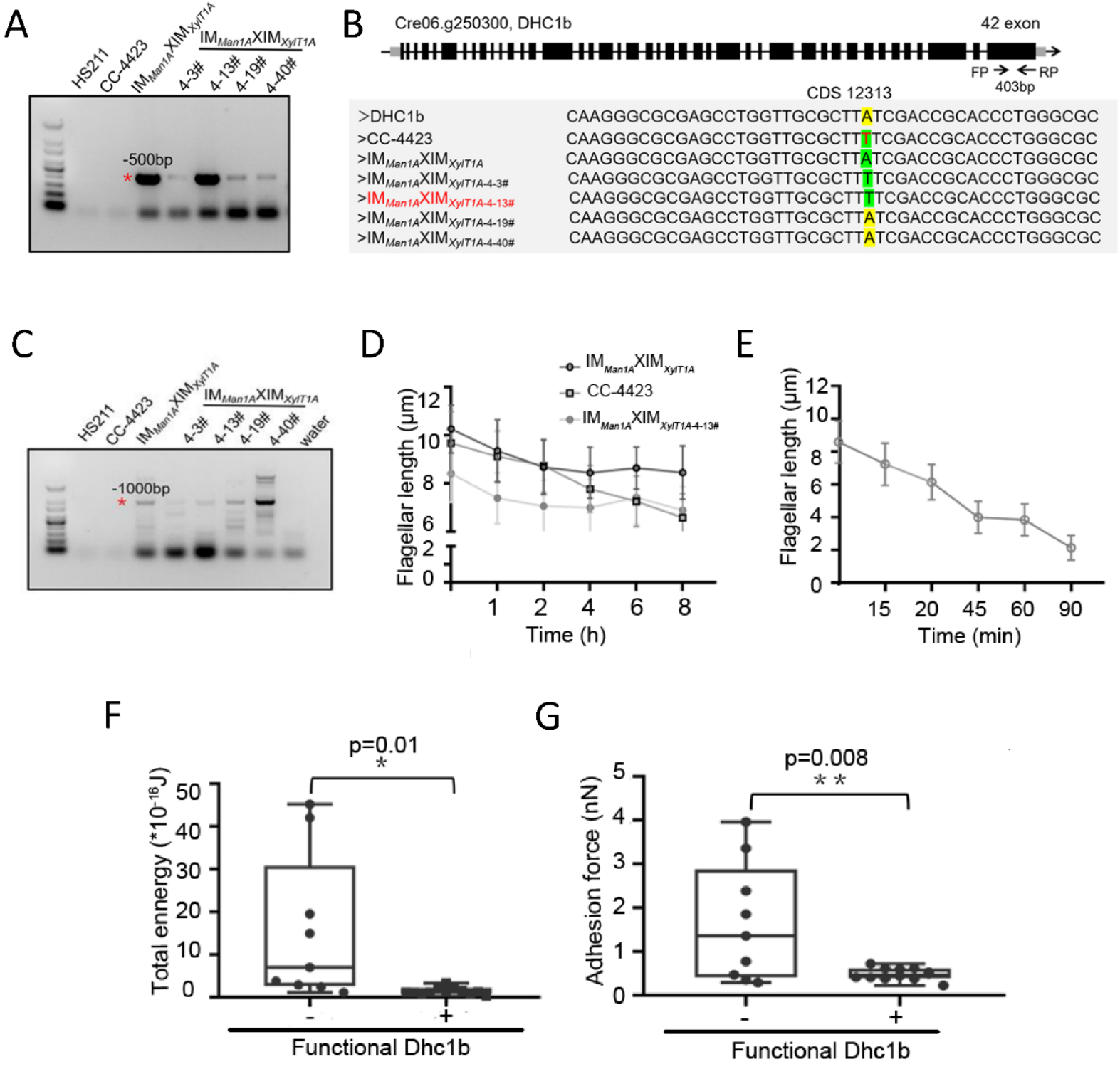
A
HS211
CC-4423
IM$_{Man1A}$XIM$_{XylT1A}$
IM$_{Man1A}$XIM$_{XylT1A}$
4-3#
4-13#
4-19#
4-40#
-500bp
B
Cre06.g250300, DHC1b
42 exon
FP
RP
403bp
CDS 12313
>DHC1b CAAGGGCGCGAGCCTGGTTGCGCTTATCGACCGCACCCTGGGCGC
>CC-4423 CAAGGGCGCGAGCCTGGTTGCGCTTTTCGACCGCACCCTGGGCGC
>IM$_{Man1A}$XIM$_{XylT1A}$ CAAGGGCGCGAGCCTGGTTGCGCTTATCGACCGCACCCTGGGCGC
>IM$_{Man1A}$XIM$_{XylT1A-4-3#}$ CAAGGGCGCGAGCCTGGTTGCGCTTTTCGACCGCACCCTGGGCGC
>IM$_{Man1A}$XIM$_{XylT1A-4-13#}$ CAAGGGCGCGAGCCTGGTTGCGCTTTTCGACCGCACCCTGGGCGC
>IM$_{Man1A}$XIM$_{XylT1A-4-19#}$ CAAGGGCGCGAGCCTGGTTGCGCTTATCGACCGCACCCTGGGCGC
>IM$_{Man1A}$XIM$_{XylT1A-4-40#}$ CAAGGGCGCGAGCCTGGTTGCGCTTATCGACCGCACCCTGGGCGC
C
HS211
CC-4423
IM$_{Man1A}$XIM$_{XylT1A}$
IM$_{Man1A}$XIM$_{XylT1A}$
4-3#
4-13#
4-19#
4-40#
water
-1000bp
D
IM$_{Man1A}$XIM$_{XylT1A}$
CC-4423
IM$_{Man1A}$XIM$_{XylT1A-4-13#}$
Flagellar length (μm)
Time (h)
E
Flagellar length (μm)
Time (min)
F
p=0.01
*
Total ennergy (*10^{-16}J)
Functional Dhc1b
G
p=0.008
**
Adhesion force (nN)
Functional Dhc1b

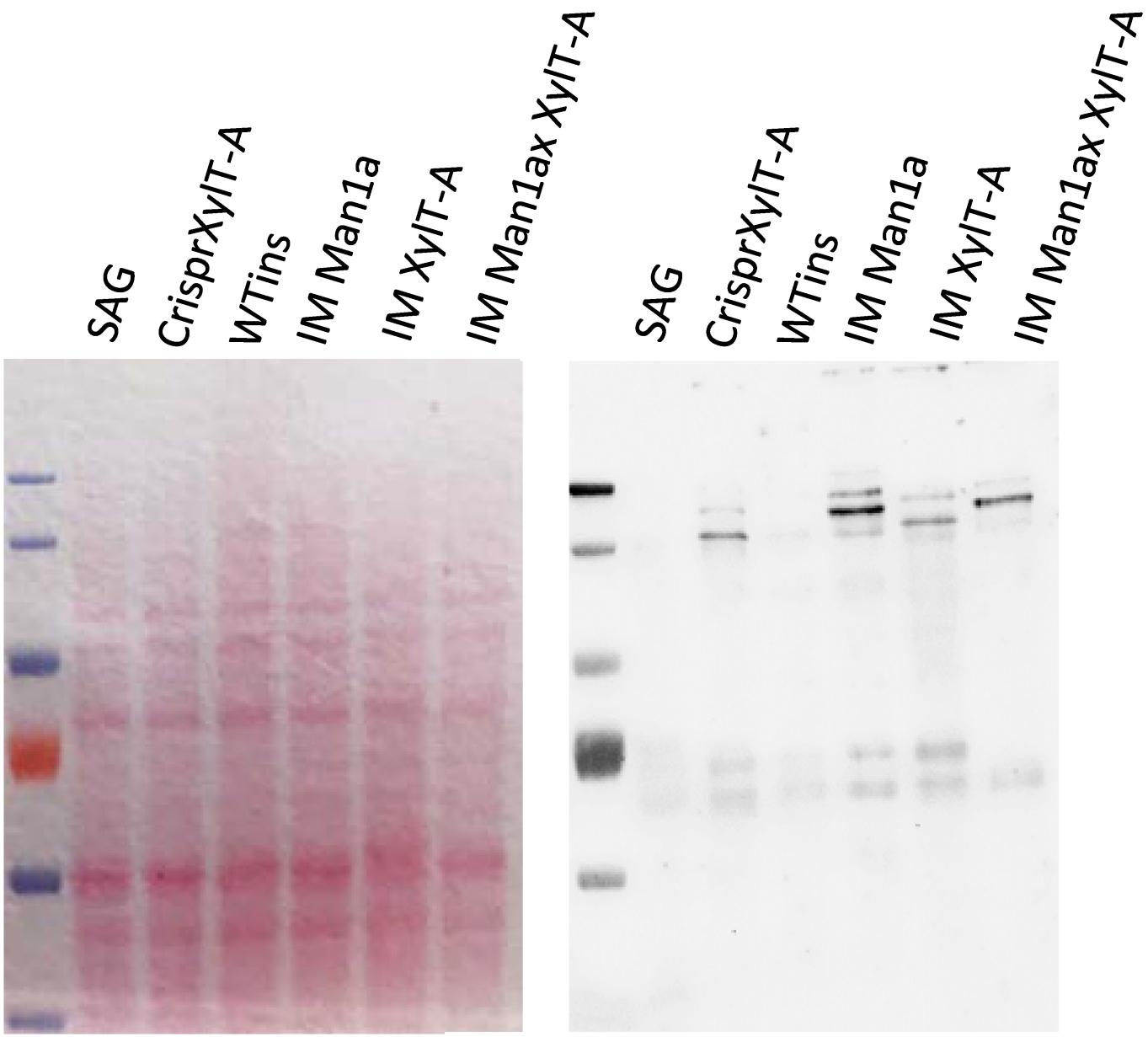
SAG
CrisprXylT-A
WTins
IM Man1a
IM XylT-A
IM Man1ax XylT-A
SAG
CrisprXylT-A
WTins
IM Man1a
IM XylT-A
IM Man1ax XylT-A

40µg